Title
EXPERIMENTAL STUDY OF P AND l?p INTERACTIONS IN THE RANGE 1 - 10 GeV/c

Author
Hauptman, J.M.

Publication Date
1977

Submitted to Nuclear Physics B

LBL-5541
Preprint

EXPERIMENTAL STUDY OF Λp AND $\bar{}^{o}p$ INTERACTIONS IN THE RANGE 1 - 10 GeV/c

J. M. Hauptman, J. A. Kadyk, and G. H. Trilling

January 1977

Prepared for the U. S. Energy Research and
Development Administration under Contract W-7405-ENG-48

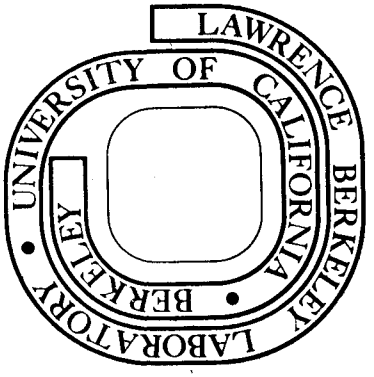

DISCLAIMER

LBL-5541

EXPERIMENTAL STUDY OF Λp AND $\Xi^{o}p$ INTERACTIONS IN THE RANGE 1 - 10 GeV/c*

J. M. Hauptman,** J. A. Kadyk, and G. H. Trilling

Lawrence Berkeley Laboratory and Department of Physics
University of California, Berkeley, California 94720

ABSTRACT

The reactions $\Lambda p \rightarrow \Lambda p$, $\rightarrow \Sigma^{\pm} p \pi^{\mp}$, $\rightarrow \Lambda p \pi^{+} \pi^{-}$ and $\rightarrow \Sigma^{o} p$ have been studied in the SLAC 82-inch bubble chamber for incident Λ particles in the momentum range 1 - 10 GeV/c. The incident Λ flux was produced by the exposure of a platinum target mounted inside the chamber to a 12-GeV K^{-} beam. A total of 992 events have been analyzed. The reactions are found to be qualitatively similar to corresponding nucleon-nucleon reactions. In particular, the slope parameter, B, in the elastic cross section $\frac{d\sigma}{dt} = Ae^{Bt}$ has been determined as a function of incident momentum and found to be consistent with that for proton-proton elastic scattering. Angular distributions for the inelastic channels are compared with those of similar nucleon-nucleon reactions, and predictions of relevant exchange models.

---

*Work supported by the U. S. Energy Research and Development Administration.

**Present address: Department of Physics, University of California, Los Angeles, CA 90024.

I. INTRODUCTION

The interactions of pions, kaons and nucleons with protons have been extensively studied and analyzed in the momentum range below 20 GeV/c. By comparison very little is known about the hyperon-proton interactions, primarily because of the shortness of the hyperon lifetimes, which correspond to decay pathlengths of a few centimeters for hyperon momenta of several GeV/c. An improvement on the relatively modest sample of hyperon-proton interactions requires a substantial increase in one or more of the following factors: the integrated hyperon flux, the density of hydrogen or the hyperon decay length. Since the mean decay length is proportional to the momentum, the available decay lengths are limited by the energy region under study. It is not known how to appreciably increase the density of hydrogen over that available in a liquid hydrogen target or a bubble chamber. Hence, the only reasonable possibility appears to be the first: either longer experiments, higher fluxes or both.

In the experiment described here, a technique is used which enhances the flux of Λ particles. A beam of high-energy K^- particles strikes a platinum-plate target mounted inside a large, hydrogen bubble chamber. The hyperons produced inside the target by K^--Pt nucleus interactions usually emerge into the bubble chamber volume where they can be observed to interact occasionally with protons. The K^- interactions in the complex nucleus frequently produce Λ particles ($\sigma(K^- p \rightarrow \Lambda + \text{anything}) \cong 1.8$ mb). In addition, other hyperons will, as a result of intra-nuclear collisions, often produce Λ particles as well. Among the stable hyperons, the Λ has a relatively long lifetime and has two other properties making it an attractive choice for experimental investigation: it exists in a pure $I = 0$ state, and the Λ decay $\Lambda \rightarrow p\pi^-$ is especially well-suited to experimental identification and measurement.

In order that the produced Λ emerge from the target with high probability, it is necessary that the target thickness be small compared with a decay length. We chose to study Λp interactions above 1 GeV/c, since the range below 1 GeV/c has been previously investigated [1]. These goals were achieved in the present experiment by use of a 12-GeV/c K^- beam at SLAC, striking a platinum target of one interaction length thickness mounted inside the SLAC 82-inch hydrogen bubble chamber [2]. The resulting Λ momentum spectrum has a mean of 2.2 GeV/c, corresponding to a 15-cm decay length. Hence, about 75% of the produced Λ's escaped from the plate before decaying. The relatively high momentum of the Λ would not be expected from peripheral production in K^--nucleon collisions, but at such high energies as these the production of Λ's is dominated by high multiplicity reactions, which are in turn associated with nonperipheral behavior [3].

Below is a list of the reactions analyzed in this paper along with the number of events of each type:

Reaction	Number of events	
$\Lambda p \rightarrow \Lambda p$ (elastic)	584	(1)
$\Lambda p \rightarrow \Sigma^- p\pi^+$	132	(2)
$\Lambda p \rightarrow \Sigma^+ p\pi^-$	60	(3)
$\Lambda p \rightarrow \Lambda p\pi^+\pi^-$	181	(4)
$\Lambda p \rightarrow \Sigma^0 p$	35	(5)
various $\Xi^0 p$ interactions	25	

II. EXPERIMENTAL TECHNIQUES

A. Data Collection

The experiment consists of 500,000 photographs with a platinum plate target mounted in the central plane of the chamber. The plate was 3 inches

thick in the beam direction, 10 inches wide (horizontally) across the chamber, and 3/4 inch high. The beam was altered somewhat from its usual optical configuration in order to obtain a K^- beam image at the plate only 3/8 inch high, and about 6 inches wide.

The plate was mounted downstream of the entrance window, so that about 2 - 3 inches of beam track was visible upstream of the plate; this permitted the vertex of the K^- interaction, which is the Λ origin, to be reconstructed from the incident beam track as well as from outgoing secondary tracks emerging from the plate. A large horizontal dispersal of the beam at the plate was found to be important in avoiding confusion from adjacent tracks in origin reconstruction, and in reducing the general background of secondary tracks immediately downstream from the plate. There were on the average about 6 beam tracks per picture, of which about 4.5 were K^- and the remainder were μ^- and π^-. A decay $\Lambda \rightarrow p\pi^-$ was seen about every 5 pictures, and during the course of the experiment about 150,000 Λ were produced and entered the visible region. All but about 2% of these decayed without interacting with a proton in the liquid hydrogen. A sample of 7% of these free decays were used to determine the Λ beam flux and momentum spectrum. In the present experiment, a broad spectrum of Λ momentum results from production in the platinum plate, as shown in fig. 1. This spectrum was used to obtain the cross sections for reactions (1) - (5).

The identification of specific reactions relies upon kinematic reconstruction of the event, since signatures from the film scan, such as ionization, decays, etc., are not always present, and usually contain a selection bias. The reactions (1) - (4) which supplied most of the events in the present analysis belong to the highest constraint class, and the background from topologically similar reactions was small.

The origin of the incident Λ in the platinum is

determined from incoming and outgoing charged tracks so that the only quantity not directly measured is the magnitude of the Λ momentum. Reactions (1) - (4) are overconstrained by three kinematic equations, and are called three-constraint (3C) fits. Reaction (5) has only one constraint (1C) but there are very few ambiguities with other reactions of similar topology, providing the incident Λ momentum is below about 1.5 GeV/c. For about 25% of the events, the origin did not reconstruct well, and the loss of the incident Λ direction measurement reduces the events from reactions (1) - (4) to the one-constraint (1C) class, and such events from (5) cannot be analyzed. The total number of Λp events analyzed is 992, which represents about one-third of all Λp interactions observed. Thus, the unanalyzed Λp reactions, which generally lie in lower constraint classes due to one or more neutral secondary particles, constitute a background from which the reactions (1) - (5) must be separated.

About 65% as many $K^o_S \rightarrow \pi^+\pi^-$ decays are observed as $\Lambda \rightarrow p\pi^-$ decays, and the $K^o_L p$ interactions contribute a non-negligible background in the selection of Λp interactions, especially for the less well-constrained reactions. However, for the more highly constrained reactions (1) - (4) this background is small compared with the statistical uncertainty, and is not a serious problem in the analysis.

An appreciable number of hyperons other than Λ emerge from the plate. Relative to the Λ flux, the following hyperon fluxes are observed in the chamber: $\Sigma^{\pm}(\sim 0.1)$, $\Xi^-(0.015)$ and $\Omega^-(0.0002)$. The Ξ^- and Ω^- are observed with relatively high efficiency by virtue of their decay to Λ particles, and are found to have average momenta somewhat higher than that for the Λ: Ω^-(4.7 GeV/c), Ξ^-(3.7 GeV/c), cf. Λ(2.2 GeV/c). The charged Σ hyperons are much more difficult to find in scanning, being detected only by the change of track direction as the incident hyperon decays to the secondary: $\Sigma^{\pm} \rightarrow \pi^{\pm} n$, or

$\Sigma^+ \rightarrow p\pi^o$. The decay angles are quite small for the high momenta considered here, and Σ^- interactions and decays are easily confused with similar reactions induced by K^- beam particles. For these reasons, an analysis of the $\Sigma^{\pm}p$ interactions was not done. A small number of $\Xi^o p$ interactions have been observed and will be discussed in Sec. IV.

B. Scanning and Measuring

The film was scanned for all interactions induced by neutral particles in which the decay of a charged or neutral strange particle was observed among the secondary particles. All of the candidate events found were carefully re-examined by a more experienced scanner to confirm their identification, and instructions for their measurement were prepared. The events were then measured using projectors with film plane digitization online to an IBM 7044 computer. In addition to measuring the tracks participating in the hyperon interaction, measurements were made of tracks associated with hyperon origins in the target. Entering beam tracks and all minimum ionizing tracks leaving the plate were measured if they were associated with an interaction in the platinum. In each view, these target-associated tracks were fit to circles which were propagated through the plate, including multiple scattering errors and energy loss correction in a search for potential Λ origin points. In the case of Λ origins resulting from beam track interactions in the liquid hydrogen, the K^- interaction point was measured in each view. These view-by-view vertex points were passed to TVGP for use in the three-dimensional reconstruction of the origin. All kinematic solutions having confidence levels greater than 1% were examined at the scan table for consistency of particle identification with bubble density information. The consistent solutions were used in the subsequent analysis.

In order to estimate the scanning efficiencies, 30% of the film was scanned

twice, and a smaller fraction was done a third time. We find an appreciable spatial variation of the scanning efficiency along the beam direction for all topologies. A drop in efficiency is observed near the plate due to obscuration by secondary particles from the K^--Pt nucleus collisions, and a somewhat smaller decrease in efficiency is seen in the downstream half of the chamber where events seldom occur. The usual assumption that each event has the same a priori probability of being found by a scanner is not a good assumption in the first few centimeters downstream of the platinum target [4]. These efficiency variations along the beam direction have been taken into account in the subsequent analysis of the data.

Certain other biases also require efficiency corrections. The elastic reaction suffers from loss of events due to the unrecognizably short recoil proton tracks at low momentum transfer (< 100 MeV/c proton momentum). This loss has been corrected by an extrapolation to $t = 0$, using the measured momentum-dependent elastic slope parameter. This correction is largest at the highest momentum, where it amounts to about 7%. The scanning efficiency for $\Sigma^{\pm}$ hyperons is biased both by the short decay length and small angle decay losses. The short decay length losses are corrected from the proper-lifetime distributions, and the small angle decay losses from a study of the center-of-mass decay angular distribution which should be isotropic. Together these corrections amount to about 15% for $\Sigma^{\pm}$ decays. The decay mode $\Sigma^+ \rightarrow p\pi^o$ is not used in any cross-section determination because of its low detection efficiency due to the small angle decay.

The fiducial volume for all primary and secondary (decay) vertices was taken to be 40 cm in x (perpendicular to beam and camera axis), 156 cm in y (along beam direction), and 21 cm in z (along camera axis, chamber depth) inside the 82-inch hydrogen bubble chamber.

C. Background

Sources of background result from other reactions incorrectly fitting one of the reactions (1) - (5). The event giving the incorrect fit may be produced by an incident $\bar{K}^o$, an incident fast neutron, or an incident Λ. There is little ambiguity between $K_S^o \rightarrow \pi^+\pi^-$ and $\Lambda \rightarrow p\pi^-$ decays, so that backgrounds result mainly from misidentification of charged secondary particles and a kinematic overlap with reactions similar in topology to (1) - (5), but having one or more π^o's. For reactions (1) - (4) backgrounds are small because of their high constraint class, 3C. Reaction (5) is a 1C fit, but the resolution is sufficient to separate it well from the background for incident Λ momentum less than about 1.5 GeV/c, the only region where the cross section appears to be substantial for (5). Monte-Carlo simulation of various potential background reactions has confirmed that very few will make successful fits to reactions (1) - (5).

Cross sections were determined from the sample of successfully fitted events, suitably corrected for efficiencies and escape loss as discussed above, by normalization to the pathlength of the incident Λ beam.

D. The Incident Λ Spectrum

The determination of cross sections requires an accurate knowledge of the flux of the incident Λ beam:

$$\sigma = \frac{N}{L} \frac{A}{\rho N_o}$$

where N = number of events (corrected), N_o = Avogadro's number, A = atomic weight of H, ρ = hydrogen density, and L = total Λ pathlength. Here the flux is contained in the factor L. The quantities σ, N and L are all functions of the Λ momentum, p. The distribution, L(p), of pathlength as a function of momentum is obtained by summing the Λ decay lengths for all observed free decays within each interval $(\Delta p)_i$,

$$L_i(p_i) = \sum_{j=1}^{N_i} \lambda_j(p_i) \quad ,$$

where the sum is over the N_i events in the momentum interval $(\Delta p)_i$ centered at p_i. This is equivalent to obtaining the spectrum of Λ momentum, dN/dp, and multiplying by the corresponding decay lengths.

The spectrum, and hence the pathlength distribution, was determined by measuring a small fraction, 0.0667, of free Λ decays, sampled uniformly throughout the data. These decays were fitted to the 1C hypotheses $\Lambda \rightarrow p\pi^-$, $K^o_S \rightarrow \pi^+\pi^-$, and $\gamma \rightarrow e^+e^-$. The resulting Λ momentum and pathlength distributions are shown in figs. 1a-b. These distributions are also corrected for scanning and measuring efficiencies, K^o_S-Λ kinematic ambiguities, and the branching ratio for the visible decay mode,

$$R(\Lambda \rightarrow p\pi^-) = 0.64 \quad .$$

The pathlength distribution in fig. 1a has been scaled from the sampling fraction to give the total Λ pathlength observed in the experiment.

III. Λp INTERACTIONS

A. Elastic Scattering, $\Lambda p \rightarrow \Lambda p$

The elastic cross section for Λp scattering has gross features similar to either pp or np elastic scattering. This cross section is displayed in fig. 2 in seven momentum intervals of equal Λ pathlength over the range from 0.4 to 10 GeV/c. The differential elastic cross sections $\frac{d\sigma}{d\Omega}$ and $\frac{d\sigma}{dt}$ are displayed in fig. 3 as functions of incident Λ momentum, and one may note, in particular, the rapid variation in shape of the distribution in $\cos\theta^*$ as the elastic reaction proceeds from nearly isotropic to highly peripheral scattering. Fits of the differential cross section in t to the form

$$\frac{d\sigma}{dt} = Ae^{Bt} \quad , \quad 0.01 \leq -t\,(\mathrm{GeV/c})^2 \leq 0.41$$

exhibit a shrinkage of the elastic diffraction peak very similar in both magnitude and momentum dependence to that observed in pp elastic scattering. These fitted slope parameters are shown in fig. 4, together with pp slope parameters fitted by the same algorithm over the same range of t. Care has been taken in the determination of the Λp slope parameters to avoid a kinematic bias which can be introduced by averaging data over a finite range in Λ center-of-mass momentum. The bias is a result of the cos θ^* distribution being mapped onto different regions of t for different center-of-mass momenta. We have corrected for this by transforming t_i for each event in a given Λ momentum bin by the Jacobian of the transformation relating cos θ^* to t:

$$t_i' = t_i\left(\frac{q_o}{q_i}\right)^2$$

where q_i is the center-of-mass momentum of that event, and q_o an appropriate average over the momentum bin, $q_o = \frac{1}{n}\sum_{i=1}^{n} q_i$. It is clear from fig. 4 that within errors the Λp and pp slopes are in agreement. These results are also compatible with those of ref. [2].

The polarization of the final state Λ in the elastic reaction has been measured over the center-of-mass angular range $0.30 \leq \cos\theta^* \leq 0.95$ by using the known decay asymmetry of the Λ, and the results are shown in fig. 5. The Λ polarization is found to be small and consistent with zero. Averaged over the range 1 - 4 GeV/c, the Λ polarization is $\langle P \rangle = 0.03 \pm 0.12$. By contrast, the proton polarization in pp elastic scattering is 0.20 - 0.40 in the 1 - 4 GeV/c range as shown in fig. 5, and the corresponding average for protons is 0.28 [5]. A possible explanation of this difference in behavior is contained in the model of Arnold and Logan [6], which predicts that the primary contribution to NN polarization is due to A_2, and not ω, exchange interference with the pomeron. Since the isospin singlet nature of the Λ forbids A_2 exchange in the elastic reaction, this model would suggest a suppression of the Λ polarization.

The question of cusp-like or resonant behavior in this cross section near the threshold for the reaction $\Lambda p \rightarrow \Sigma^{o} p$ has been of some interest since the original paper of de Swart and Dullemond [7], and later analyses by the same group. However, in the present data there seems to be no evidence for such effects, as can be seen from fig. 6.

B. $\underline{\Lambda p \rightarrow \Sigma^{\pm} p \pi^{\pm}}$

The $\Sigma p \pi$ reactions (2) and (3) are the simplest inelastic Λp interactions in the 3C constraint class, and measured cross sections for these are shown in figs. 7a and 7b.

Reactions (2) and (3) are especially interesting for potential insight into the mechanisms of inelastic Λp processes. Some of these expected to be present are indicated by figs. 8a-g. Since the Σ^{-} has an isospin of unity, one expects pion exchange to play a prominent role in reaction (2), as, for example, in fig. 8e. This should result in strong Δ^{++} formation as well as peripheral production of the Σ^{-}. Similar behavior is expected for Σ^{+}, reaction (3), fig. 8a, except that here the Δ^{o} is formed with a weaker coupling than was the Δ^{++} in reaction (2). Figures 9a and 9b show the square of the effective masses for the baryon-pion combination, and figs. 10a and 10b give the angular distributions of the Σ. These distributions generally fulfill the expected behavior.

As indicated by figs. 8b and 8f, a Y^{*} resonance may be formed at the top vertex from exchange of either isospin zero or one. Although the $(\Sigma^{-}\pi^{+})$ mass plot seems to show a peak in the vicinity of 1400 MeV, this is probably a reflection of the Δ^{++}, and there is no conclusive evidence for Y^{*} production. However, some appreciable amount of Y^{*} production cannot be excluded by these results.

K or K^{*} exchange would result in backward production of Σ (see figs. 8c-d

and 8g). However, as can be readily seen, this would constitute a double charge exchange in the case of reaction (2) (fig. 8h), and is presumably suppressed. However, there is no such inhibition for reaction (3) (fig. 8d), and this fact may explain the suggestion of a backward peak in this reaction which is absent for reaction (2).

Reaction (2) may be mediated by the same exchanges as the pp reaction

$$pp \rightarrow np\pi^+ \quad . \tag{6}$$

In particular, a Δ^{++} may be formed at one vertex by π exchange, while only much weaker resonance production can occur at the other vertex (figs. 8e-f). A comparison of the cross sections for these is made in fig. 7a. The cross section for the pp reaction has been scaled by a normalization factor 0.18 obtained from a fit to the ratio of these cross sections at the same final state Q-value. The comparison was done in this way to help remove kinematic effects near threshold due to the Λ-Σ mass difference. The general shapes of the plots are seen to agree well.

The relative magnitude of the cross sections are related by SU(3) couplings, $\Lambda\Sigma\pi$ and $NN\pi$, at the upper vertex, the lower vertex being dominated by Δ^{++}. While the former is purely symmetric, the latter has mixed symmetry, and the relative amount of each coupling is related to the ratio of cross sections as

$$\left.\frac{\sigma(\Lambda p \rightarrow \Sigma^- \Delta^{++})}{\sigma(pp \rightarrow n\Delta^{++})}\right|_{\pi \text{ exchange}} = \frac{2}{3}(1 - f)^2 \quad ,$$

where $f = \frac{F}{F + D}$ is the ratio of antisymmetric to (symmetric plus antisymmetric) couplings. A calculation of f from the best fit for the ratio of cross sections gives

$$f = 0.48 \pm 0.07 \quad .$$

This value is in reasonably good agreement with several other determinations [8], as indicated in fig. 11.

A similar comparison between reaction (3) and $np \rightarrow pp\pi^-$ is made in fig. 7b. Here several exchanges may contribute to comparable degrees, and it does not seem possible to make a convincing argument about the exchange mechanism. However, as indicated in fig. 7b, the cross section for $np \rightarrow pp\pi^-$ seems to agree well in shape with the cross section for reaction (3).

Angular distributions of the Jackson angle, $\cos\alpha$, and the Treiman-Yang angle, φ, for $\Lambda p \rightarrow \Sigma^-\Delta^{++}$ are shown in fig. 12. Although it is clear that neither distribution agrees well with predictions for pure pion exchange, there are similarities between the distributions for reaction (2) and the corresponding pp reaction [9] shown as dashed curves.

C. $\Lambda p \rightarrow \Lambda p\pi^+\pi^-$

The cross section for the two-pion production reaction (4), $\Lambda p \rightarrow \Lambda p\pi^+\pi^-$, is displayed in fig. 13, in which the solid curve superposed is a representation of the $np \rightarrow np\pi^+\pi^-$ cross section obtained from the literature. These two cross sections are equal, within experimental uncertainty, at all momenta from threshold to 10 GeV/c.

This reaction proceeds partly through the quasi-two-body process:

$$\Lambda p \rightarrow \Sigma_{1385}\Delta_{1236} \ .$$

This may be seen by examining the $(\Lambda\pi)$ and $(p\pi)$ invariant mass distributions in figs. 14 and 15. For incident Λ momentum of 3 - 5 GeV/c, where reasonable statistics are available, an analysis of these mass distributions has been made assuming that they are a sum of a Lorentz invariant phase space and a p-wave Breit-Wigner for each of the Σ_{1385} and Δ_{1236} resonant states. Estimates of the relative contribution of each of these parts was obtained, and the solid lines of fig. 16 are the result of these determinations. The lower curve on each plot is the contribution of phase space alone, and the upper curve is the sum of phase space and the fitted Breit-Wigner. The results of these fits are given in table 1.

In addition to the mass distribution analyses of the preceding paragraphs, we have examined the hypothesis that the reaction (4) proceeds by single pion exchange. The Gottfried-Jackson and Treiman-Yang angular dependences at the $p\pi\Delta$ vertex, agree reasonably well with this hypothesis, as is seen in fig. 17. With the exception of the point at $\cos\alpha \approx -1.0$, the experimental distributions follow closely the expected ones:

$$|\psi(\cos\alpha)|^2 \propto 1 + 3\cos^2\alpha$$

and

$$|\psi(\varphi)|^2 \propto \text{constant} \quad .$$

These results show that the double pion production reaction $\Lambda p \rightarrow \Lambda p\pi^+\pi^-$ is qualitatively similar to double pion production in nucleon-nucleon scattering in cross section, resonance production, and single pion exchange characteristics.

D. $\Lambda p \rightarrow \Sigma^0 p$

The cross section for reaction (5) rises sharply above threshold (P_Λ = 0.642 GeV/c) to a peak of about $\sim 8-10$ mb (at $P_\Lambda \sim 0.85$ GeV/c), and then falls rapidly. This result agrees with that of an earlier experiment, as may be seen in fig. 18. Although this reaction is not highly constrained (1C at the production vertex), there are very few ambiguous events for $P_\Lambda \lesssim 1.5$ GeV/c, and we believe that the background is small.

A comparison can be made between the cross-section for reaction (5) and the reaction

$$\Sigma^- p \rightarrow \Lambda n$$

by assuming SU(2) invariance and detailed balance to transform to the equivalent Λ momentum. Such a comparison is shown in fig. 18, and there is seen to be only crude agreement between the different experiments [9], the $\Sigma^- p$ data lying systematically lower in the region of the peak.

In fig. 19 is shown the production angular distribution for reaction (5). Here we have included data from an earlier Λp experiment [10], and the Λ momentum

has been restricted to lie below 1.0 GeV/c, to show the strong effect of partial waves higher than S-wave entering, even close to threshold. The shape of this distribution suggests the presence of an appreciable P-wave component.

IV. $\Xi^o p$ INTERACTIONS

Twenty-five Ξ^o interactions (table 2) have been unambiguously identified. These correspond to a cross section of about 21 mb averaged over the Ξ^o momentum range from 1.5 to 12 GeV/c. This cross section estimate was made assuming that both the number and spectrum of Ξ^o hyperons produced are the same as those for the Ξ^- hyperons observed in this experiment, and the Ξ^o pathlength distribution based on this assumption is shown in fig. 20. This Ξ^o pathlength distribution is obtained from the corresponding Ξ^- distribution by multiplying the ordinates by a factor equal to the lifetime ratio of Ξ^o and Ξ^-. Previous experiments reporting ΞN interactions at lower energies are noted in ref. [11].

The $\Xi^o p$ interactions observed which yield a final state having a Ξ^- or two hyperons are given in table 2, where the incident Ξ^o momentum is listed for each event; also, the corresponding cross sections averaged over all momenta are given. The distribution of incident Ξ^o momentum values for these events compared with the flux given in fig. 20 indicates that this part of the total cross section is roughly constant in Ξ^o momentum.

An examination of table 2 indicates that, apart from reactions such as $\Xi^o p \rightarrow \Xi^o N\pi$, our ensemble of reactions represents nearly the whole of the inelastic Ξ^o cross section in this energy region. We make this assertion on the basis of the Λp data [3] and nucleon-nucleon data in which the three- and four-pion production cross sections are only 10 - 15% of the one- and two-pion production cross sections. In addition, there are many candidates for the reactions $\Xi^o p \rightarrow Y\bar{K}N$ + pions, but this class is totally ambiguous with the class $np \rightarrow YKN$ + pions, since the K, $\bar{K}$ states both decay visibly as a

$K_1^o \rightarrow \pi^+\pi^-$. The available phase space for the former is only slightly larger than for the latter, and we have assigned these events to the np class since the n flux is much larger than the Ξ^o flux. In the Λp reactions we have found that the cross section for $\Lambda p \rightarrow \bar{K}NN$ + pions is quite small, and it is expected that the YKN final state is similarly only a small part of the $\Xi^o p$ interactions. If the missing channels $\Xi^o p \rightarrow \Xi^o p\pi^o$ and $\Xi^o p \rightarrow \Xi^o n\pi^+$ (with or without additional pions) are assumed to have cross sections roughly equal to the first two listed in table 2, then an estimate of the total inelastic $\Xi^o p$ cross section is about 25 mb from 1.5 to 12 GeV/c.

V. CONCLUSIONS

In the present experiment, we have studied the high momentum behavior of the Λp interaction in the elastic and four inelastic reactions, and have found them to be qualitatively similar to the corresponding nucleon-nucleon reactions. The differential elastic Λp cross section is very similar in shape and momentum dependence to the pp cross section, implying that the general features of the Λ-proton and nucleon-nucleon interactions are very similar. The inelastic channels proceed predominantly through single pion exchanges, and resemble corresponding nucleon-nucleon exchange processes. Finally, the $\Xi^o p$ total inelastic cross section is estimated to be approximately 25 mb.

Table 1. Momentum-averaged cross sections in the reaction $\Lambda p \to \Lambda p\pi^+\pi^-$ for incident Λ momentum 3 to 5 GeV/c.

Reaction	σ (mb)
$\Lambda p \to \Lambda p\pi^+\pi^-$	5.09 ± 1.0
$\Lambda p \to \Lambda\pi^-\Delta^{++}$	1.20 ± 0.70
$\Lambda p \to \Lambda\pi^+\Delta^{o}$	0.20 ± 1.0
$\Lambda p \to \Sigma^-_{1385} p\pi^+$	1.40 ± 0.50
$\Lambda p \to \Sigma^+_{1385} p\pi^-$	1.0 ± 0.4
$\Lambda p \to \Sigma^-_{1385}\Delta^{++}$	0.76 ± 0.35
$\Lambda p \to \Sigma^+_{1385}\Delta^{o}$	0.12 ± 0.34

Table 2. $\Xi^o p$ interactions and cross sections.

Reaction	Number of events	P_{Ξ^o} values (GeV/c)	Number corrected by SU(2)	σ (mb)
$\Xi^o p \to \Xi^- p\pi^+$	5	2.42, 2.69, 7.22 3.86, 2.65	7.5	3.1 ± 1.4
$\Xi^o p \to \Xi^- p\pi^+(n\pi^o)$	2	4.14, 3.36	3.0	1.2 ± 0.9
$\Xi^o p \to \Lambda\Lambda\pi^+$	2	2.66, 2.02	4.5	1.9 ± 1.1
$\Xi^o p \to \Lambda\Lambda\pi^+(n\pi^o)$	2	6.10, 8.87	4.5	1.9 ± 1.1
$\Xi^o p \to \Lambda\Lambda\pi^+\pi^+\pi^-$	1	4.82	2.2	0.9 ± 0.9
$\Xi^o p \to \Lambda\Sigma^+$	3	3.43, 2.22, 8.17	6.0	2.5 ± 1.5
$\Xi^o p \to \Lambda\Sigma^+(n\pi^o)$	3	5.74, 8.80, 2.17	9.0	3.7 ± 2.2
$\Xi^o p \to \Lambda\Sigma^+\pi^+\pi^-$	3	8.99, 3.98, 3.88	6.0	2.5 ± 1.5
$\Xi^o p \to \Lambda\Sigma^-\pi^+\pi^+$	3	4.71, 3.87, 6.61	4.5	1.9 ± 1.1
$\Xi^o p \to \Sigma^-\Sigma^+\pi^+$	1	4.49	2.0	1.2 ± 0.9
	25		49.2	21 ± 4

REFERENCES

[1] Previously published Λ-nucleon experiments: F. S. Crawford et al., Phys. Rev. Lett. 2 (1959) 174; G. Alexander et al., Phys. Rev. Lett. 7 (1961) 348; B. A. Arbuzov et al., JETP 15 (1962) 676; T. A. Groves, Phys. Rev. 129 (1963) 1372; L. Piekenbrock et al., Phys. Rev. Lett. 12 (1964) 625; B. Sechi-Zorn et al., Phys. Rev. Lett. 13 (1964) 282; G. Alexander et al., Phys. Rev. Lett. 13 (1964) 484; P. Beilliere et al., Phys. Letters 12 (1964) 350; V. F. Visnevskii et al., Sov. J. Nucl. Phys. 3 (1966) 511; B. Sechi-Zorn et al., Phys. Rev. 175 (1968) 1735; G. Alexander et al., Phys. Rev. 173 (1968) 1452 and Nucl. Phys. B10 (1969) 554; J. A. Kadyk et al., Nucl. Phys. B27 (1971) 13. Experiments at higher momenta are: D. Bassano et al., Phys. Rev. 160 (1967) 1239; D. Cline et al., Phys. Letters 25B (1967) 446; G. Charlton et al., Phys. Letters 32B (1970) 720; K. J. Anderson et al., Phys. Rev. D11 (1975) 473.

[2] A similar technique, using an incident proton beam has been used by K. J. Anderson et al., Phys. Rev. D11 (1975) 473.

[3] M. Aderholz et al., Nucl. Phys. B5 (1968) 606; L. K. Sisterton et al., Nucl. Phys. B6 (1968) 205.

[4] J. M. Hauptman, An Experimental Study of the Lambda-Proton Interaction, Ph.D. Thesis, LBL-3608 (1974), unpublished.

[5] The polarization is defined to be positive in the direction of $\vec{P}_{beam} \times \vec{P}_{out}$, where $\vec{P}_{beam}$ is the incident particle momentum and $\vec{P}_{out}$ is that of the outgoing particle (Λ or p) whose polarization is being measured.

[6] R. C. Arnold and R. K. Logan, Phys. Rev. 177 (1969) 2318.

[7] J. J. de Swart and C. Dullemond, Ann. Phys. 16 (1961) 263; M. M. Nagels et al., Ann. Phys. 79 (1973) 338.

[8] F. Gürsey et al., Phys. Rev. Lett. 13 (1964) 299; A. W. Martin and K. C. Wali, Nuovo Cimento 31 (1964) 1324; J. K. Kim, Phys. Rev. Lett. 19 (1967) 1074.

[9] G. Alexander et al., Phys. Rev. 154 (1967) 1284; R. Engelmann, Phys. Letters 21 (1966) 587 and University of Massachusetts Report LF174 (unpublished).

[10] J. A. Kadyk et al., Nucl. Phys. B27 (1971) 13.

[11] R. A. Muller, Phys. Letters 38B (1972) 123; R. R. A. Dalmeijer et al., Letters of Nuovo Cimento 4 (1970) 373.

FIGURE CAPTIONS

Fig. 1. (a) The Λ pathlength distribution for the entire experiment; (b) the measured Λ momentum distribution in a sample of the data.

Fig. 2. The $\Lambda p \rightarrow \Lambda p$ elastic cross section from 0.5 to 10.0 GeV/c Λ laboratory momentum. The solid line represents the proton-proton elastic cross section for comparison, and the dashed line represents the Λp elastic cross section below 0.5 GeV/c.

Fig. 3. (a) The Λp elastic differential cross section in millibarns per steradian averaged over five regions in Λ laboratory momentum; (b) the Λp elastic differential cross section in millibarns per $(\text{GeV/c})^2$ of momentum transfer squared averaged over the same five regions of laboratory momentum.

Fig. 4. The Λp elastic slope parameter B from fits of the elastic differential cross section in t to the form Ae^{Bt}, for $0.01 \leq t\ (\text{GeV/c})^2 \leq 0.41$. The pp elastic slope parameter fitted in the same manner over the same t range for data in the literature is shown for comparison.

Fig. 5. The Λp elastic polarization averaged over three regions in Λ momentum and averaged over a range in center-of-mass scattering angle in which the nucleon-nucleon polarization is large and of one sign. The solid curve is a representation of the pp elastic polarization averaged over the same angular range.

Fig. 6. The Λp elastic cross section in 100 MeV/c momentum bins at the low end of our momentum spectrum. No elastic events were observed below 300 MeV/c.

Fig. 7. (a) The $\Lambda p \rightarrow \Sigma^- p\pi^+$ cross section measured in this experiment. (b) The $\Lambda p \rightarrow \Sigma^+ p\pi^-$ cross section. The solid lines are representations of the cross sections for $pp \rightarrow np\pi^+$ and $np \rightarrow pp\pi^-$ plotted at the same Q values as the corresponding $\Lambda p \rightarrow \Sigma p\pi$ reactions. The $pp \rightarrow np\pi^+$ cross section has been scaled down by the factor $r = 0.18$ (see text).

Fig. 8. Possible exchange diagrams contributing to the reactions $\Lambda p \to \Sigma^+ p\pi^-$ and $\Lambda p \to \Sigma^- p\pi^+$, and to similar nucleon-nucleon reactions.

Fig. 9. (a) Dalitz plot for the reaction $\Lambda p \to \Sigma^- p\pi^+$. Note that the density of events in this plot would not be uniform even in the absence of resonant production since these data are summed over an incident Λ momentum spectrum which populates regions of this plot unequally; (b) Dalitz plot for the reaction $\Lambda p \to \Sigma^+ p\pi^-$.

Fig. 10. (a) Distribution of the Σ^+ production angle in the reaction $\Lambda p \to \Sigma^+ p\pi^-$; (b) distribution of the Σ^- production angle in the reaction $\Lambda p \to \Sigma^- p\pi^+$.

Fig. 11. Measurements of the ratio of the antisymmetric to the (symmetric plus antisymmetric) SU(3) couplings at the $NN\pi$ vertex from this experiment and from other previous analyses.

Fig. 12. (a) Distribution of the cosine of the Jackson angle at the $\Lambda\Sigma\pi$ vertex in the reaction $\Lambda p \to \Sigma^- \Delta^{++}_{1236}$, assuming the reaction is mediated by single pion exchange; (b) distribution of the Treiman-Yang angle for the same data. The dotted lines are representations of data obtained for the reaction $pp \to n\Delta^{++}$ at 5.5 GeV/c.

Fig. 13. Cross section for the two-pion production reaction $\Lambda p \to \Lambda p\pi^+\pi^-$. The solid line is a representation of data in the literature on the cross section for $np \to np\pi^+\pi^-$.

Fig. 14. Triangle plot of the baryon-pion mass combination $(\Lambda\pi^-)$ against the mass $(p\pi^+)$ in the reaction $\Lambda p \to \Lambda p\pi^+\pi^-$. The density of events in this plot would not be expected to be uniform even in the absence of resonant production since the distribution is summed over the Λ momentum spectrum, which populates regions of the triangle plot unequally.

Fig. 15. Triangle plot of Mass$(\Lambda\pi^+)$ against Mass$(p\pi^-)$ in the reaction $\Lambda p \to \Lambda p\pi^+\pi^-$.

Fig. 16. Baryon-pion mass spectra in the reaction $\Lambda p \to \Lambda p\pi^+\pi^-$ fit to Δ_{1236} or Σ_{1385} Breit-Wigners plus phase space, restricted to incident Λ momenta between 3.0 and 5.0 GeV/c. Curves represent phase space and (phase space + Breit-Wigner). (See text.)

Fig. 17. (a) Distribution of the cosine of the Jackson angle at the $p\pi\Delta$ vertex in the reaction $\Lambda p \to \Sigma_{1385}\Delta_{1236}$; (b) distribution of the Treiman-Yang angle for the same events. The dotted lines are the expectations of single pion exchange in the reaction.

Fig. 18. Cross section for the reaction $\Lambda p \to \Sigma^o p$. The thin-lined data are the measurements of Kadyk et al. [10], and the dashed data are the expected cross sections from measured $\Sigma^- p \to \Lambda n$ cross sections using SU(2) symmetry and the principle of detailed balance.

Fig. 19. Production angular distribution of the Σ^o in the reaction $\Lambda p \to \Sigma^o p$.

Fig. 20. Estimated Ξ^o pathlength distribution in this experiment assuming that both the number and momentum spectrum of Ξ^o are the same as those measured for Ξ^- in K^- Pt nucleus collisions at 12 GeV/c.

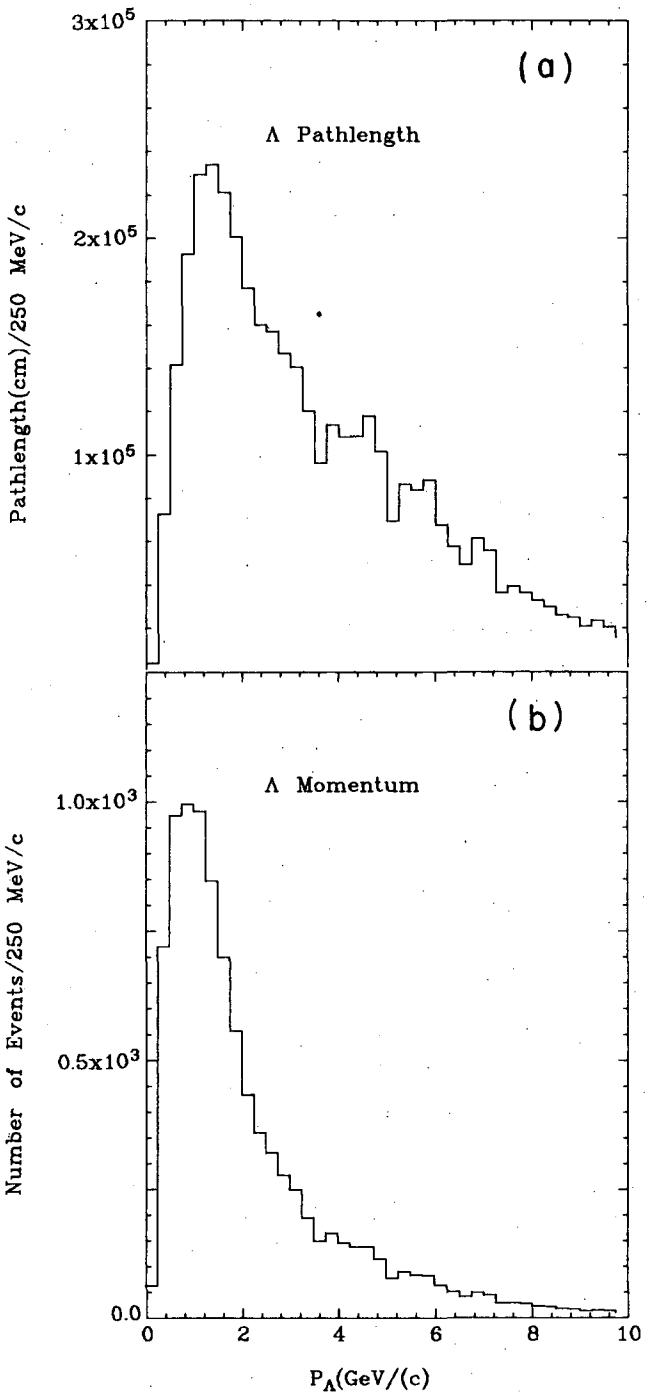

XBL 746-1065 A

Fig. 1

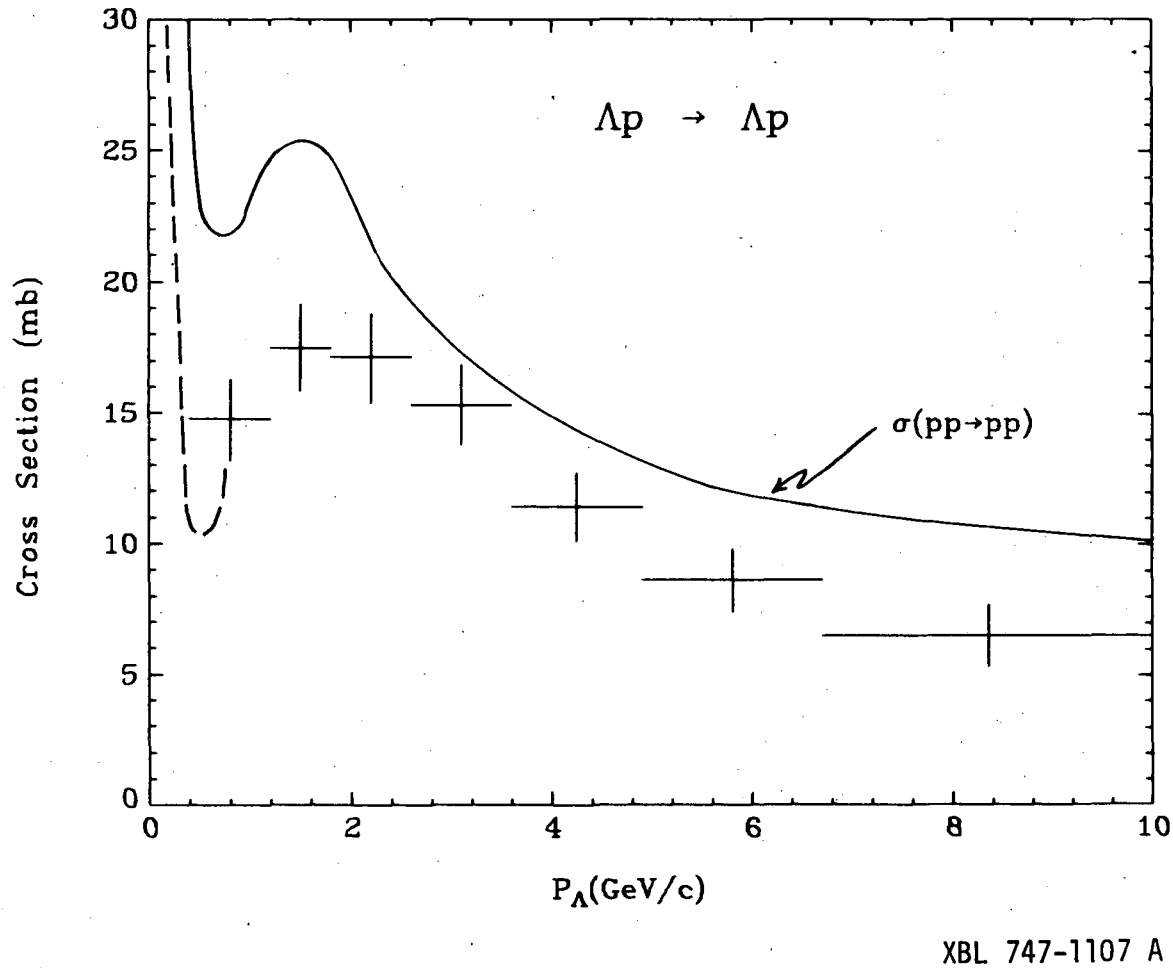
Λp → Λp
σ(pp→pp)
Cross Section (mb)
P_Λ(GeV/c)
0
5
10
15
20
25
30
0
2
4
6
8
10
XBL 747-1107 A

Fig. 2

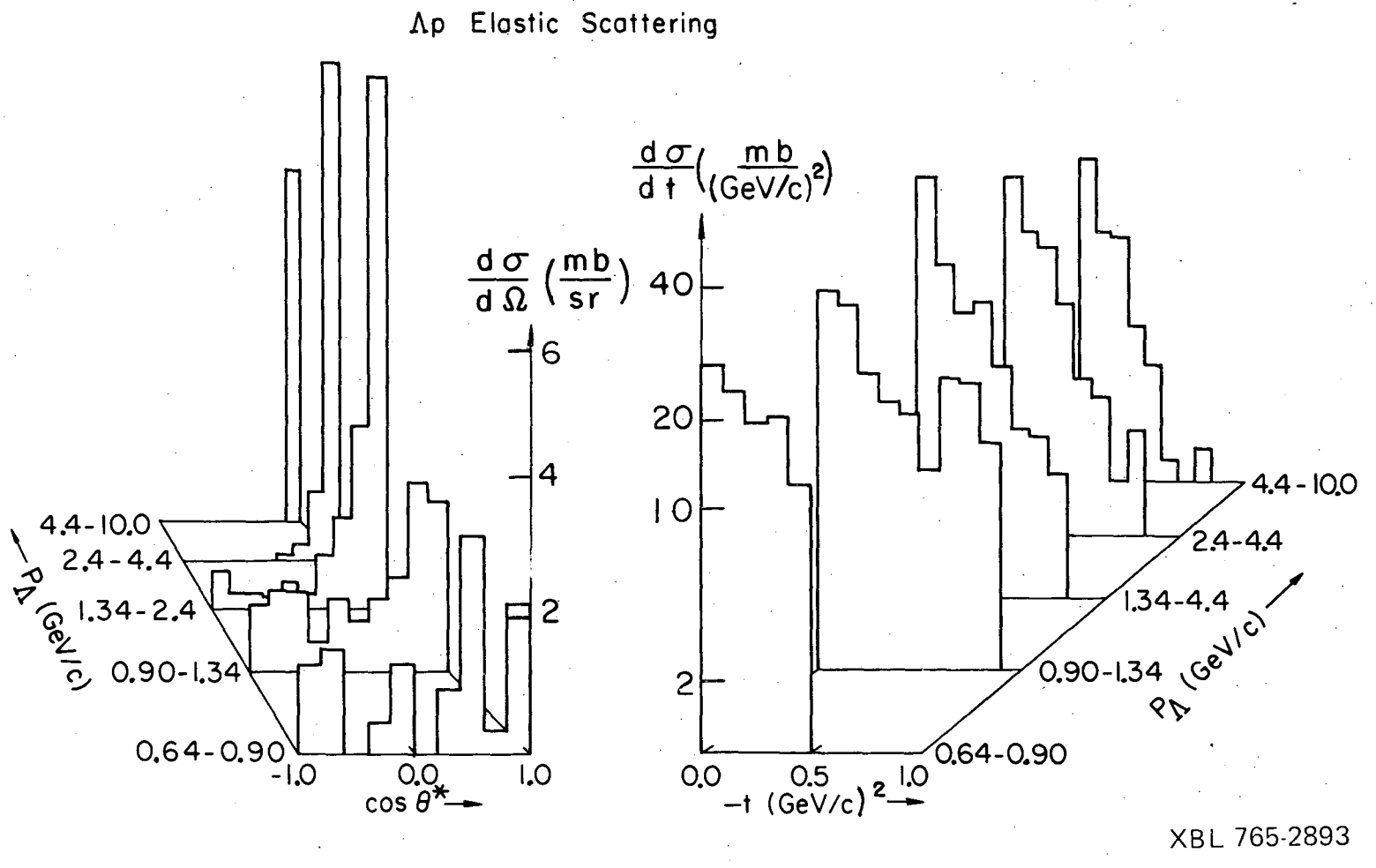

Fig. 3

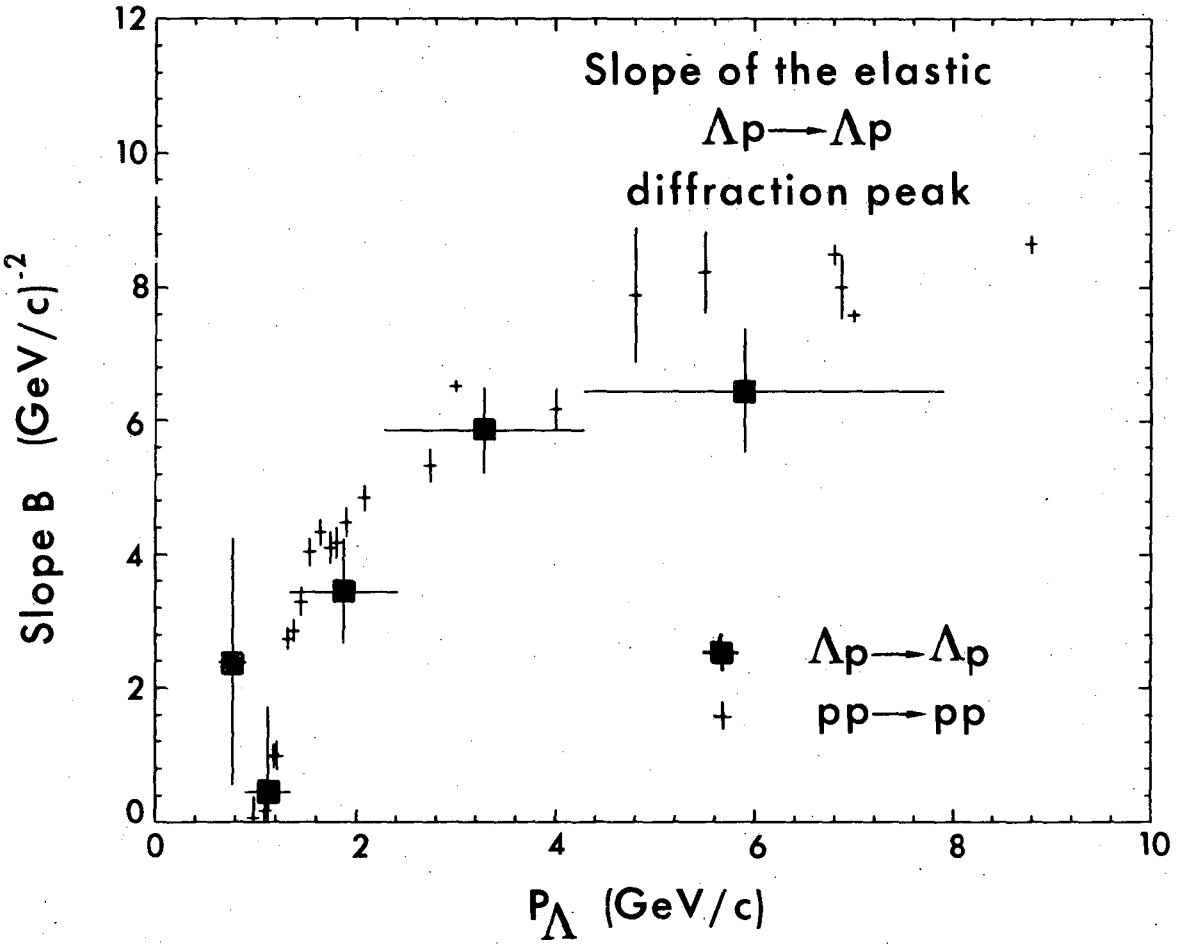
Slope of the elastic
Λp→Λp
diffraction peak
Λp→Λp
pp→pp
Slope B (GeV/c)$^{-2}$
P_Λ (GeV/c)
0
2
4
6
8
10
12
XBL 747-1106 A

Fig. 4

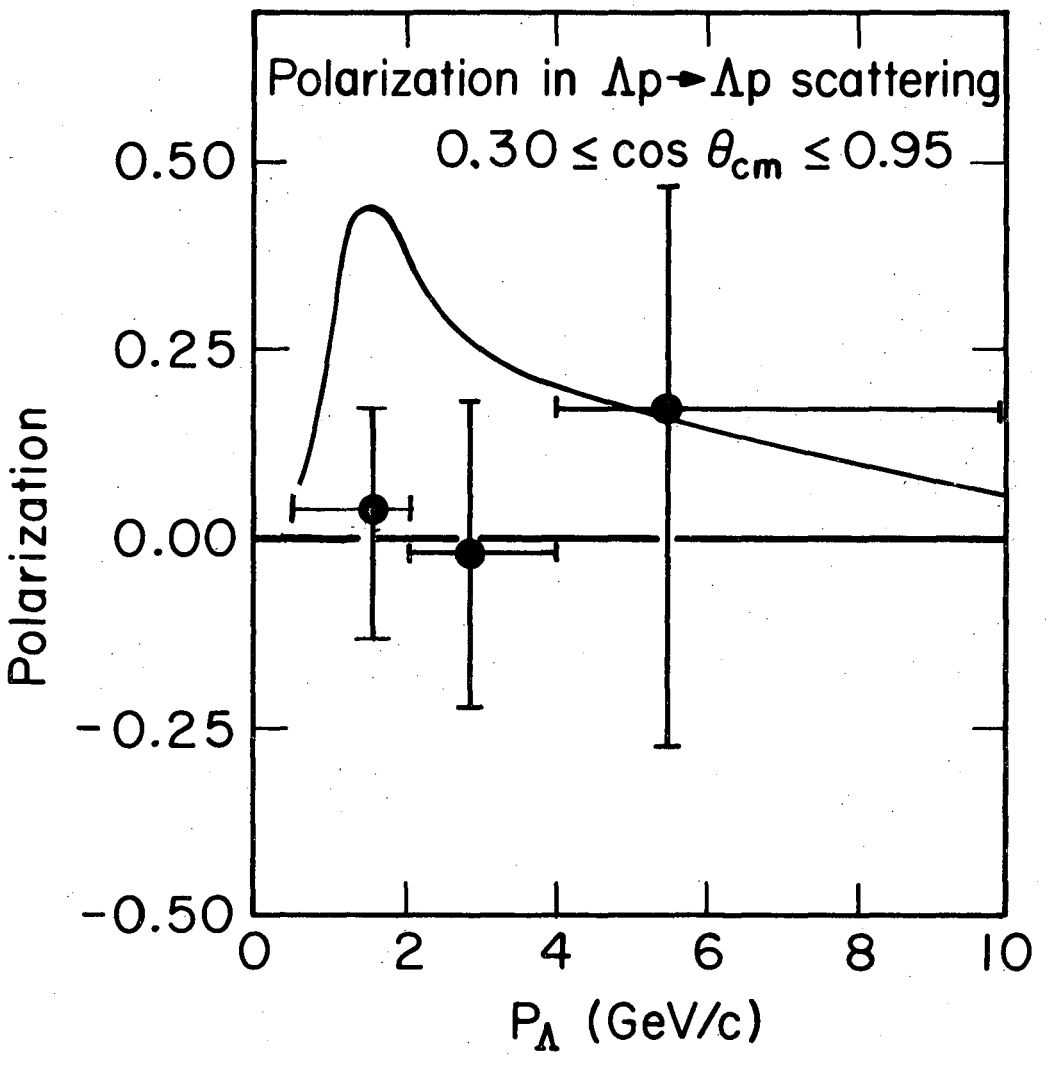

XBL 746-3517 A

Fig. 5

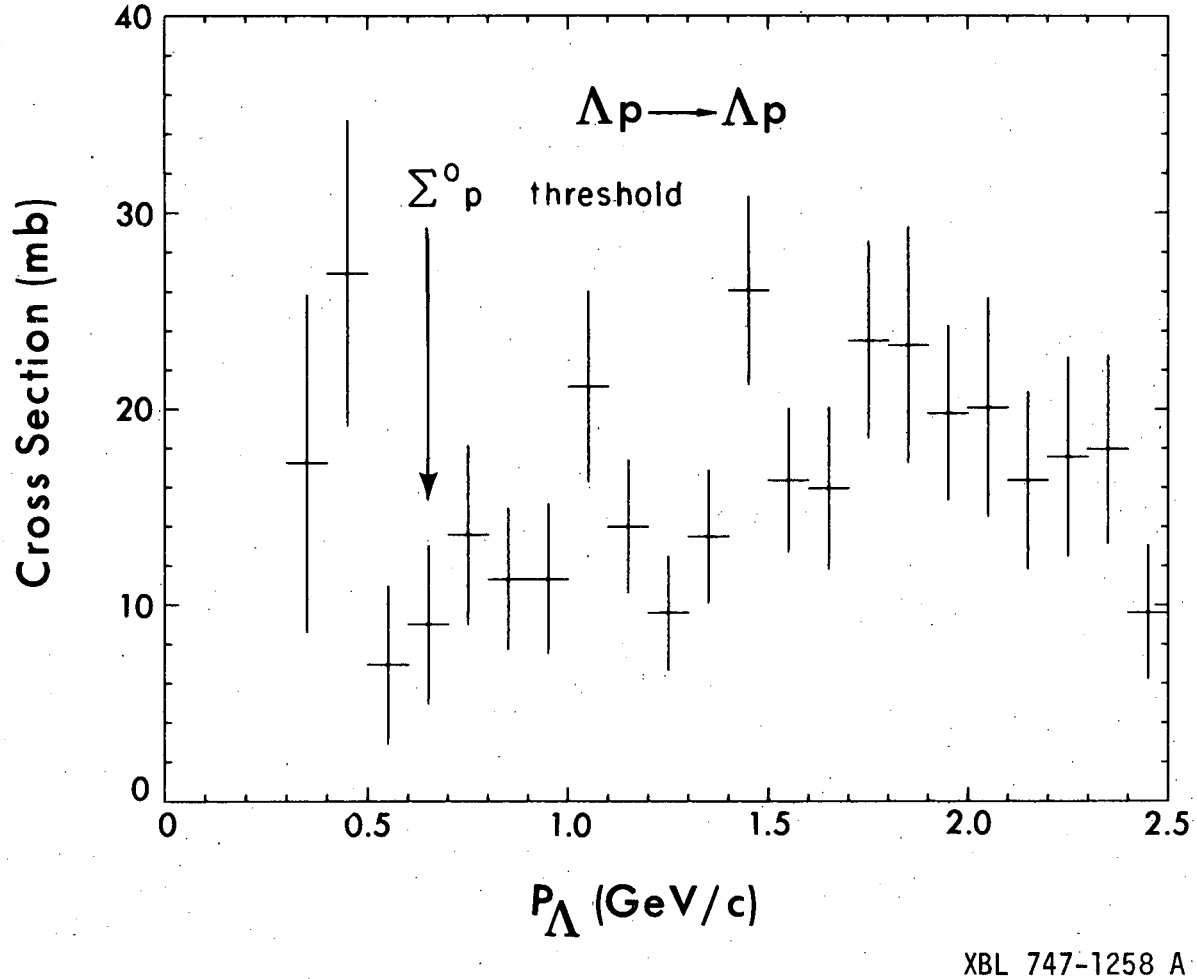
Λp⟶Λp
Σ°p threshold
Cross Section (mb)
40
30
20
10
0
0
0.5
1.0
1.5
2.0
2.5
P_Λ (GeV/c)
XBL 747-1258 A

Fig. 6

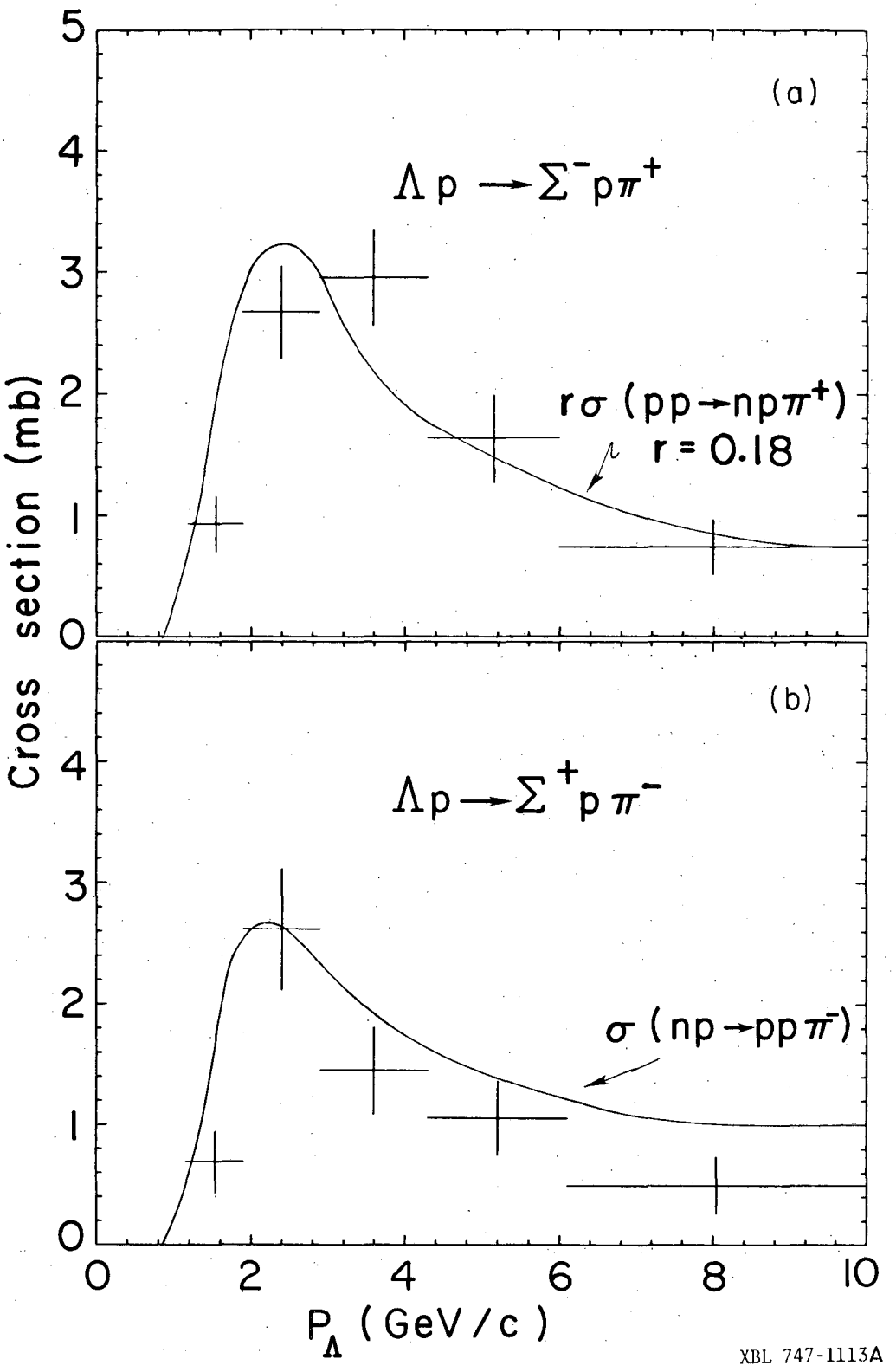

Fig. 7

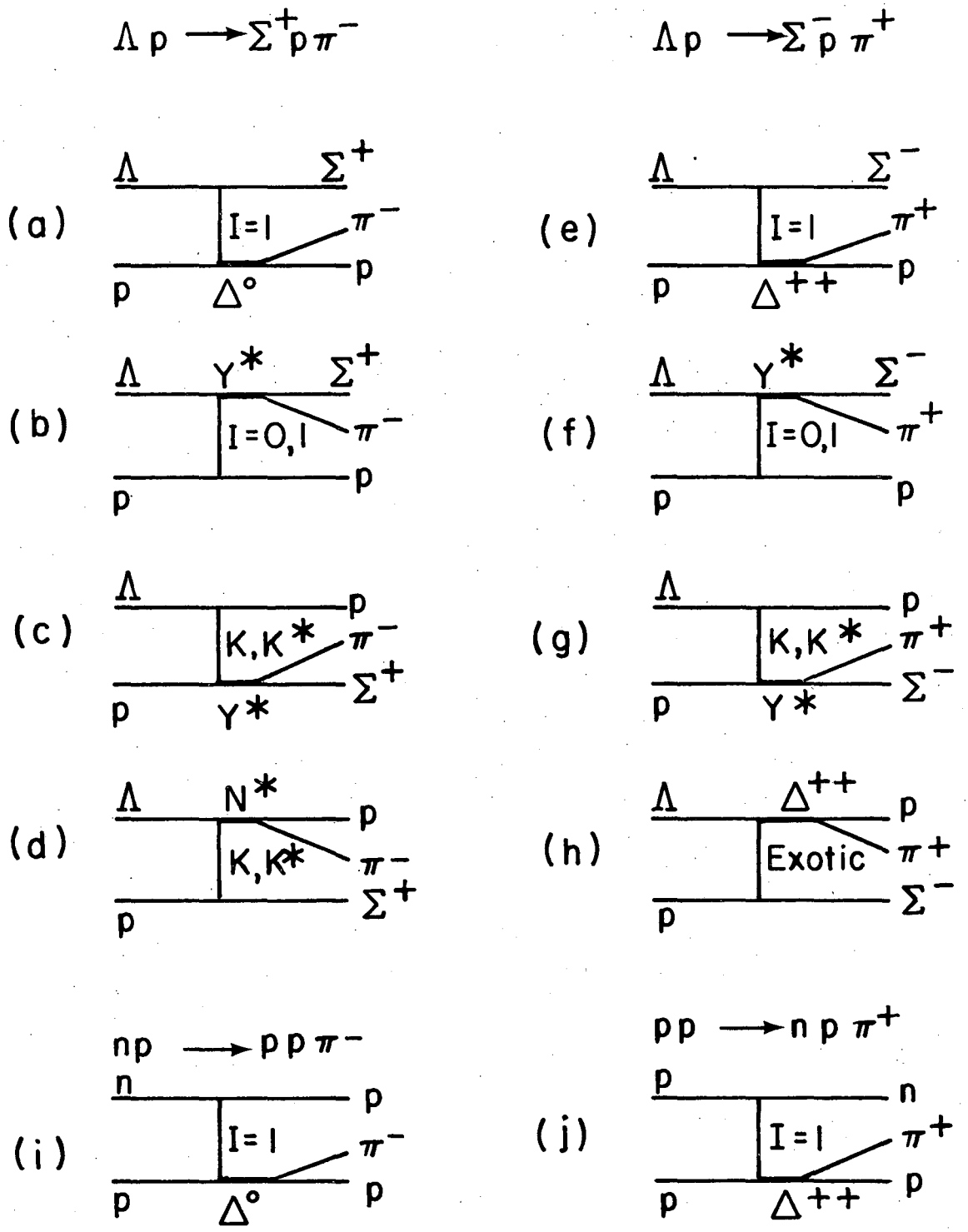
Λ p → Σ+ p π−
Λ p → Σ− p π+
(a)
Λ
Σ+
I=1
π−
p
Δ°
p
(e)
Λ
Σ−
I=1
π+
p
Δ++
p
(b)
Λ
Y*
Σ+
I=0,1
π−
p
p
(f)
Λ
Y*
Σ−
I=0,1
π+
p
p
(c)
Λ
p
K,K*
π−
Σ+
p
Y*
(g)
Λ
p
K,K*
π+
Σ−
p
Y*
(d)
Λ
N*
p
K,K*
π−
Σ+
p
(h)
Λ
Δ++
p
Exotic
π+
Σ−
p
(i)
np → p p π−
n
p
I=1
π−
p
Δ°
p
(j)
p p → n p π+
p
n
I=1
π+
p
Δ++
p
XBL765-2888

Fig. 8

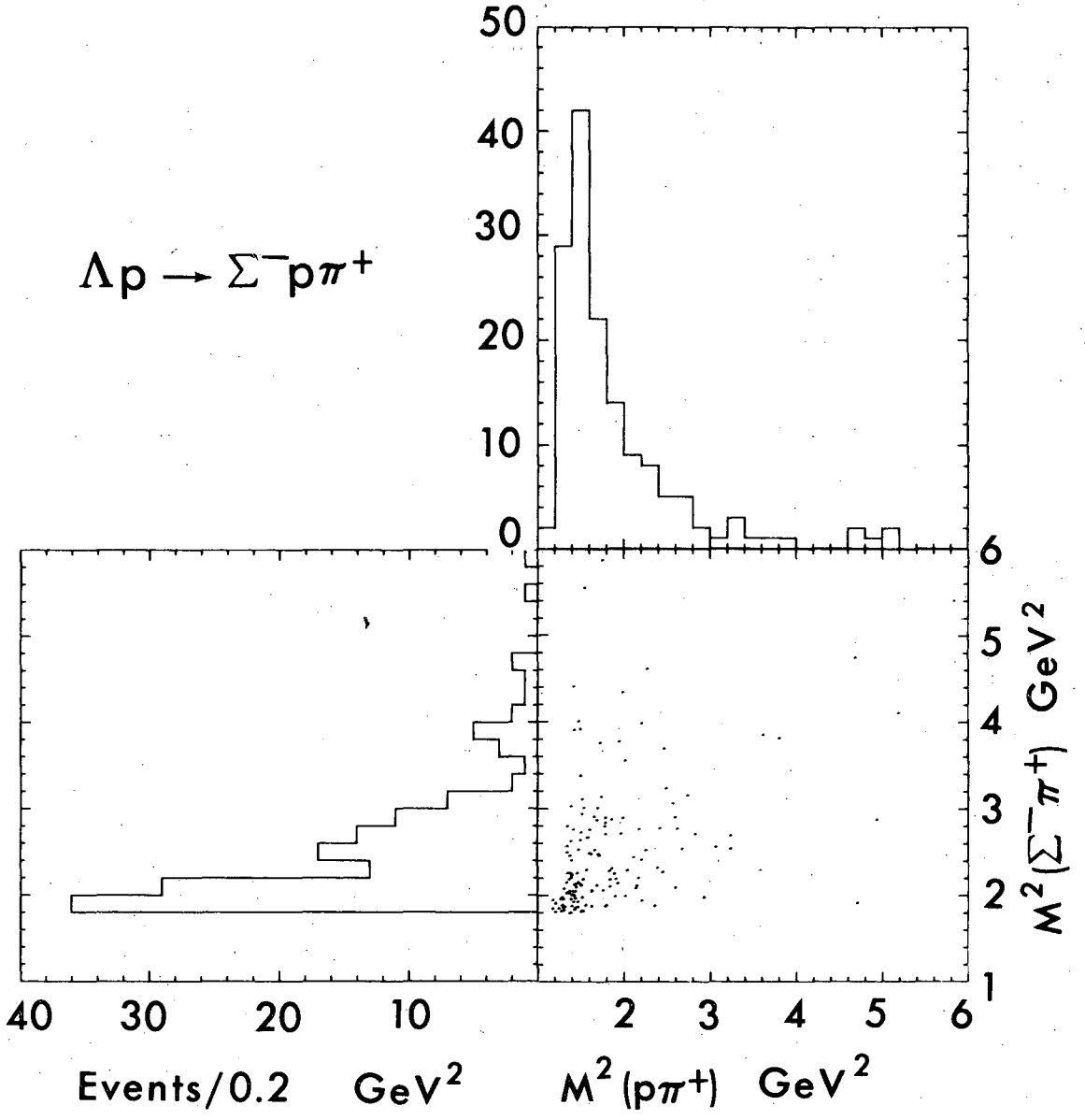

XBL 747-1112 A

Fig. 9a

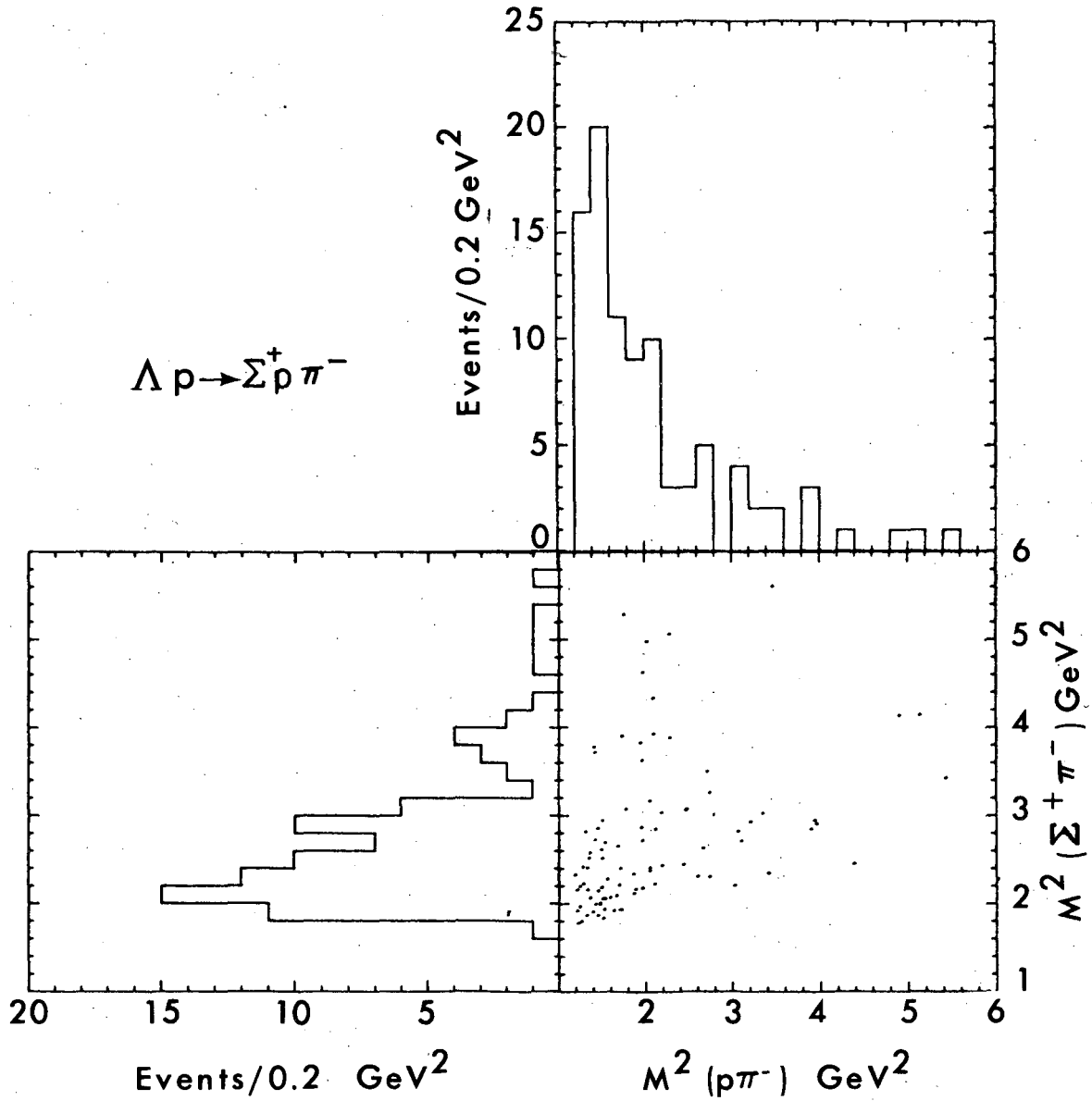
$\Lambda p \rightarrow \Sigma^+ p \pi^-$
Events/0.2 GeV^2
25
20
15
10
5
0
6
5
4
3
2
1
$M^2(\Sigma^+\pi^-)$ GeV^2
20
15
10
5
Events/0.2 GeV^2
2
3
4
5
6
$M^2(p\pi^-)$ GeV^2
XBL 747-1111 A

Fig. 9b

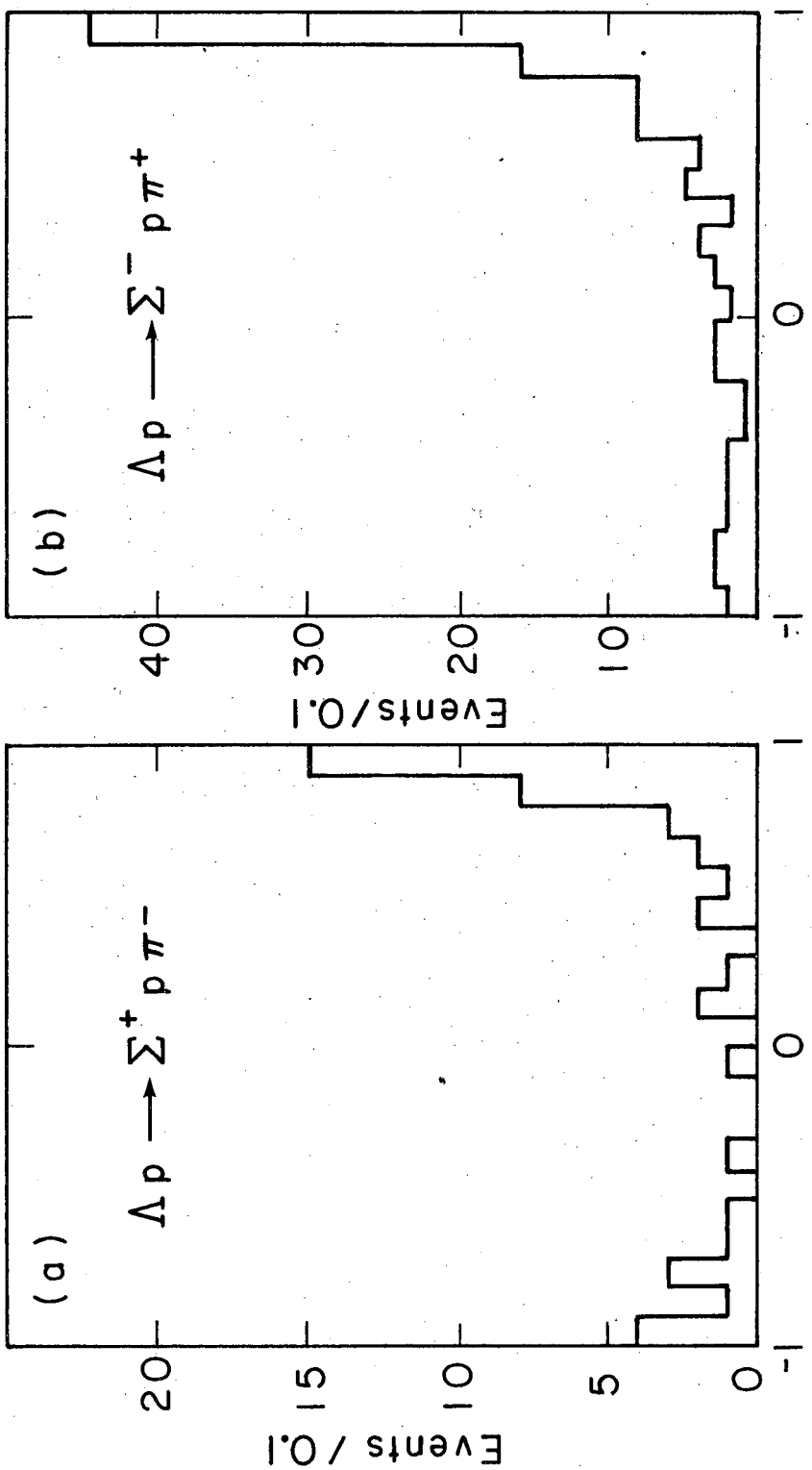

XBL 765-2891

Fig. 10

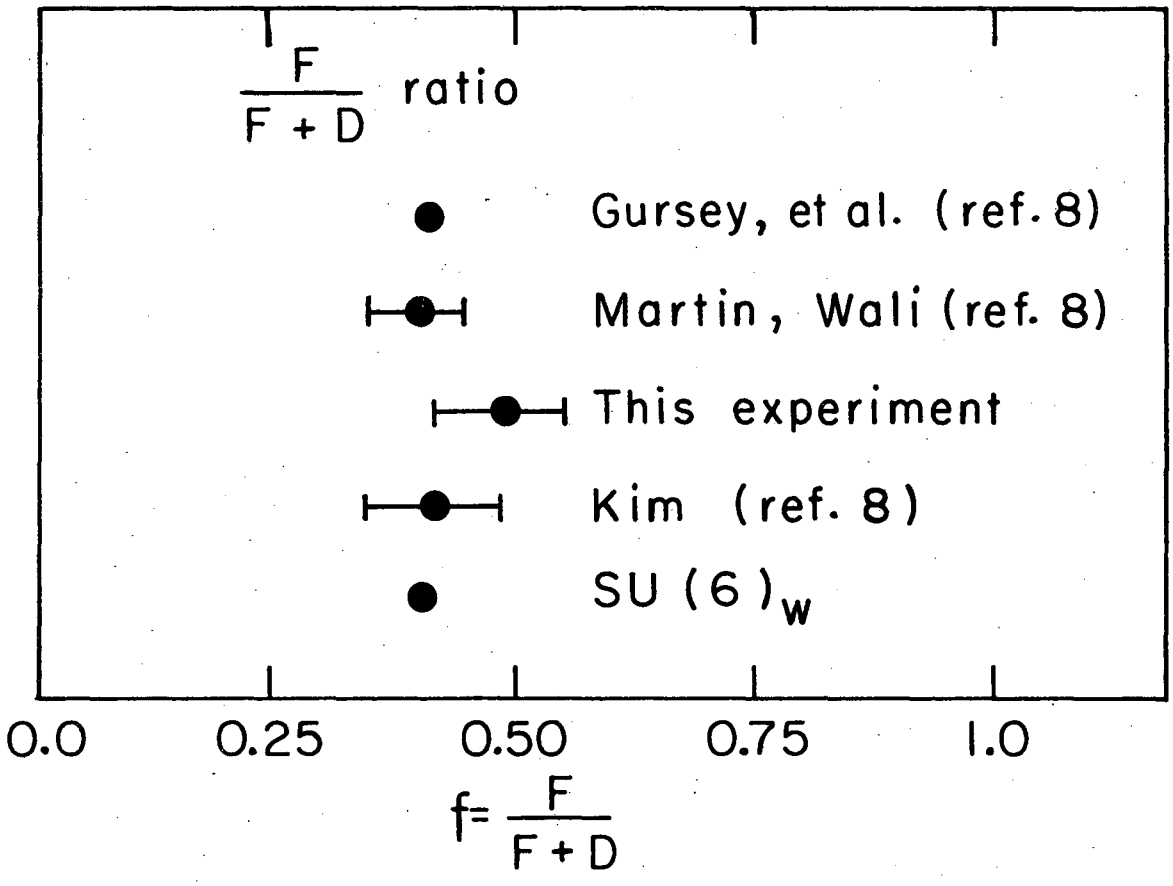

XBL 765-2890

Fig. 11

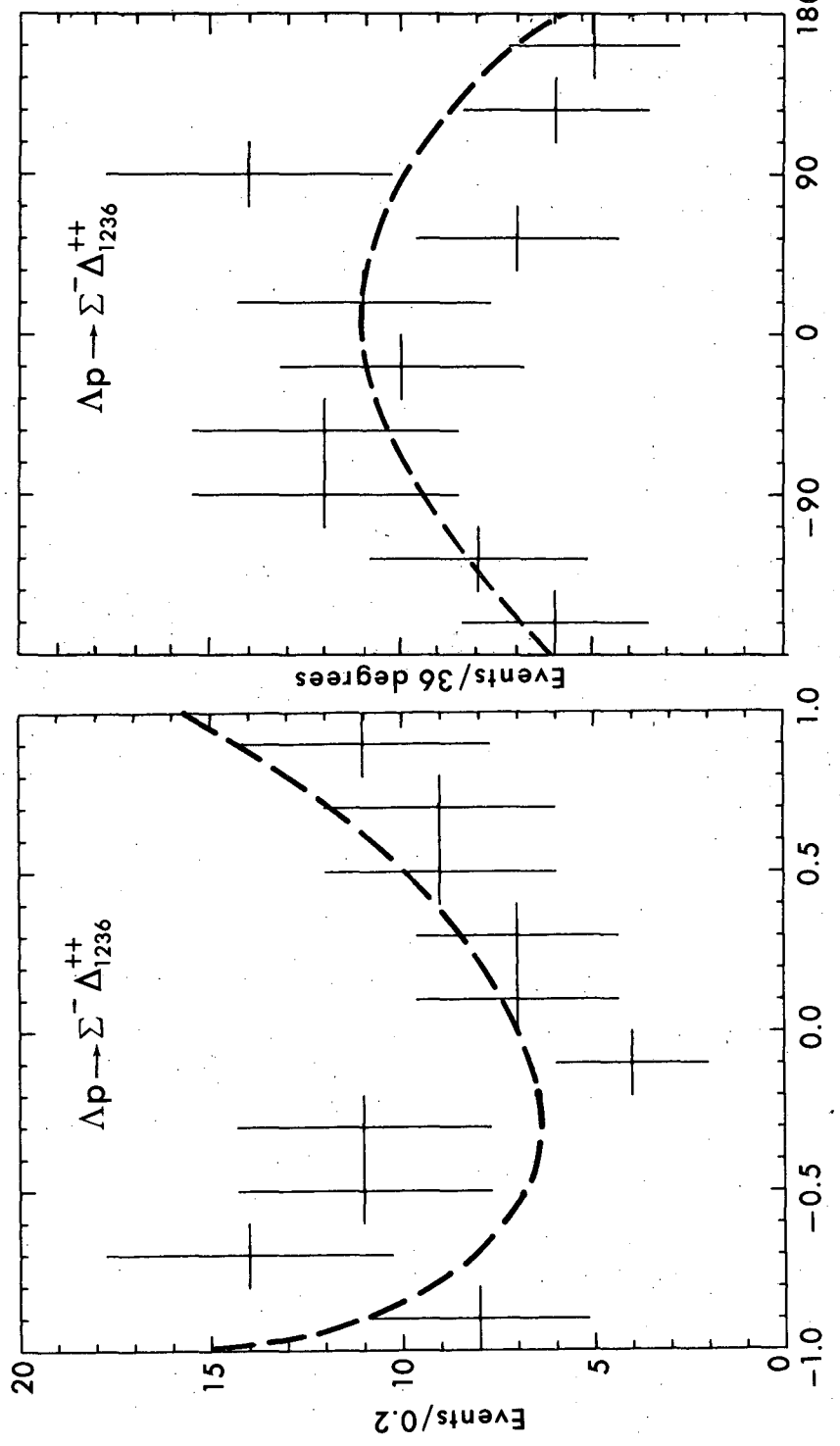

XBL 747-1115A

Fig. 12

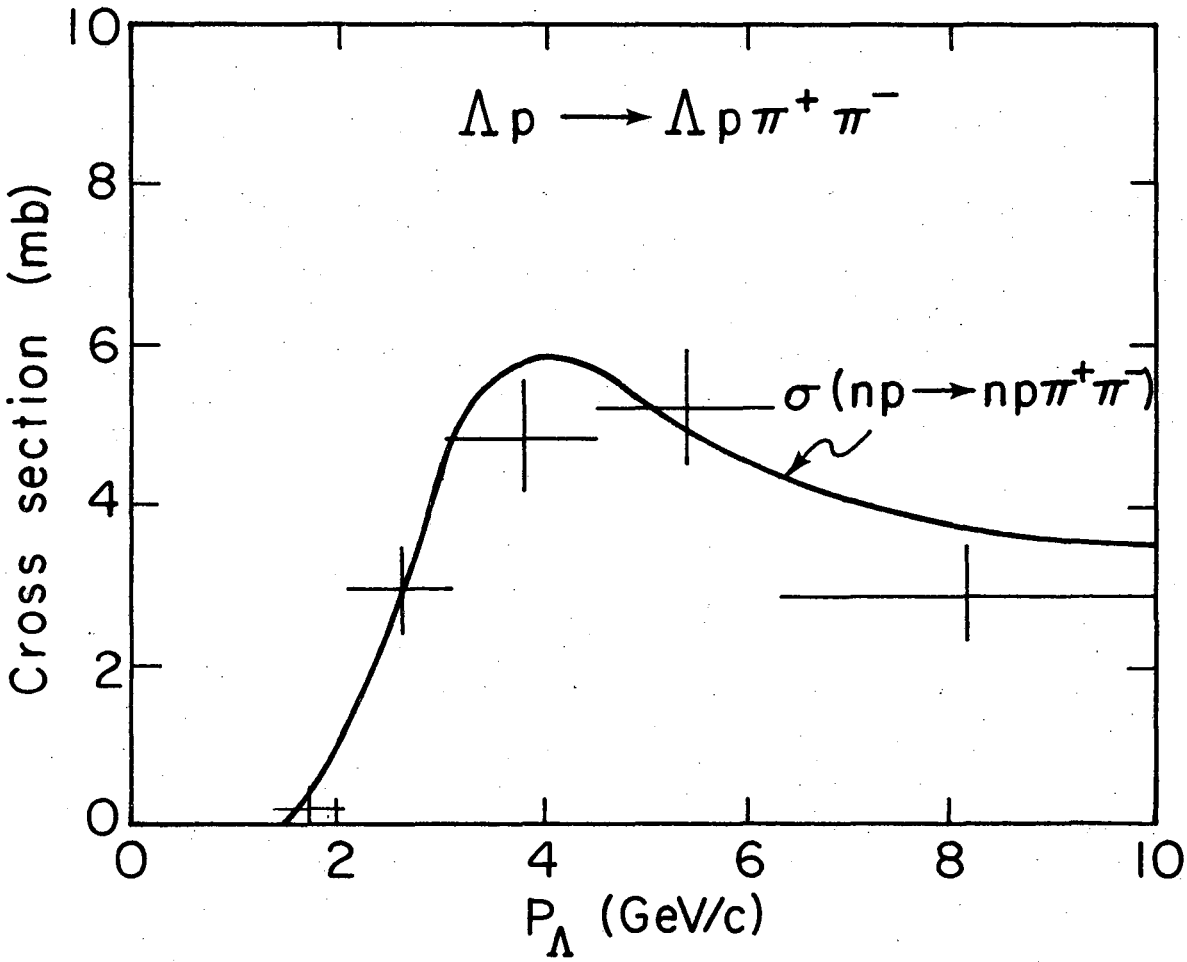

XBL 765-2892

Fig. 13

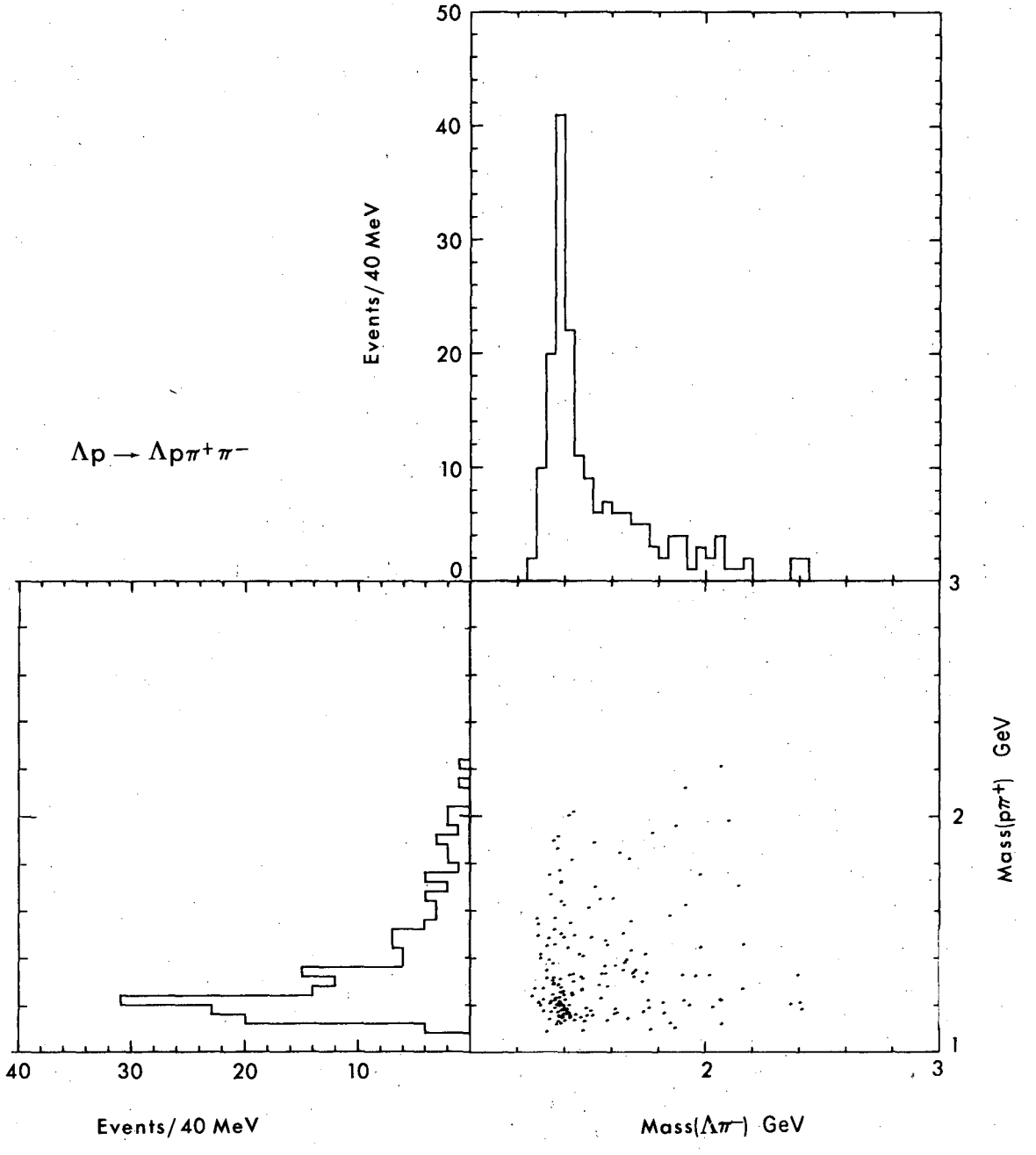

XBL 747-1110A

Fig. 14

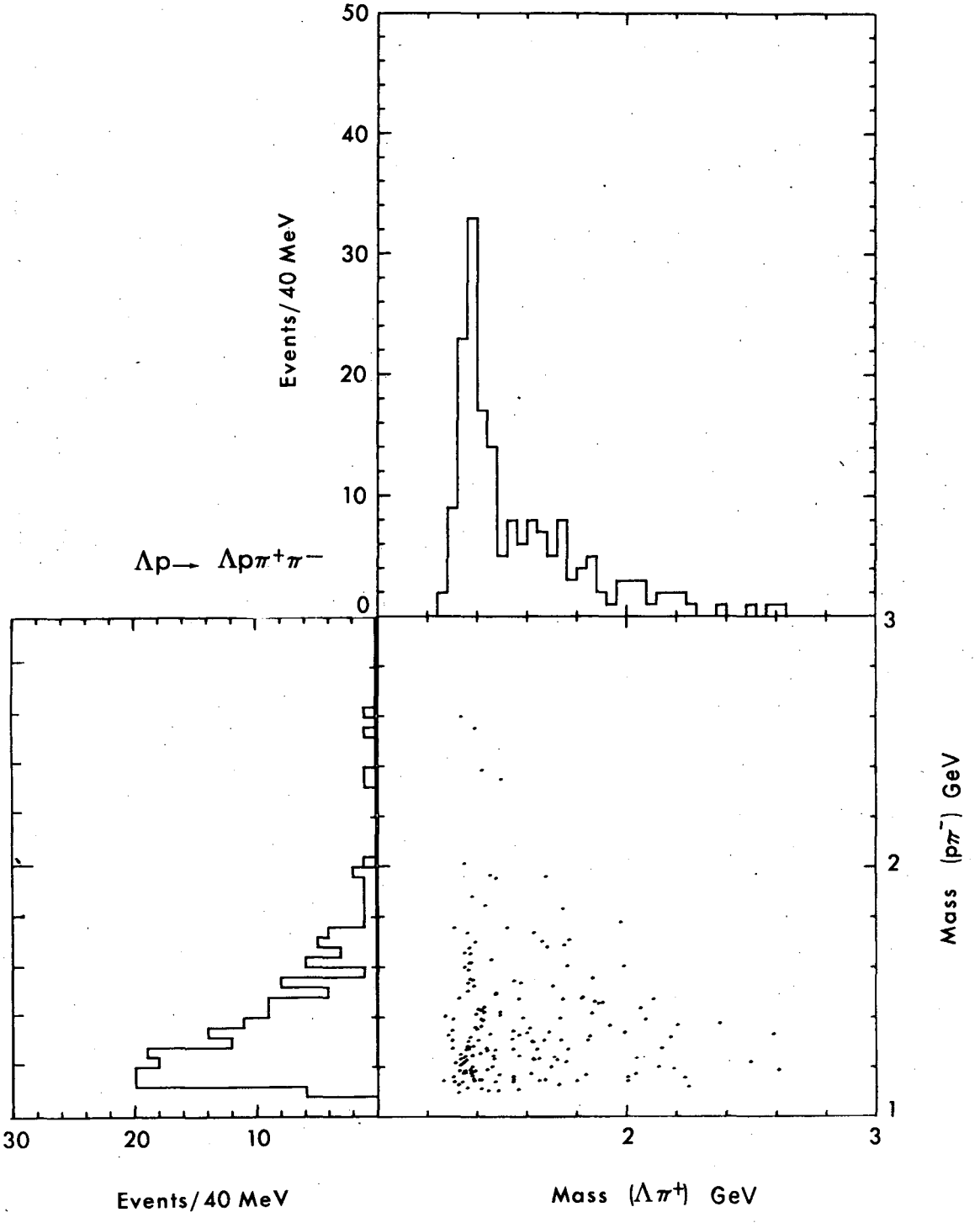

XBL 747-1109A

Fig. 15

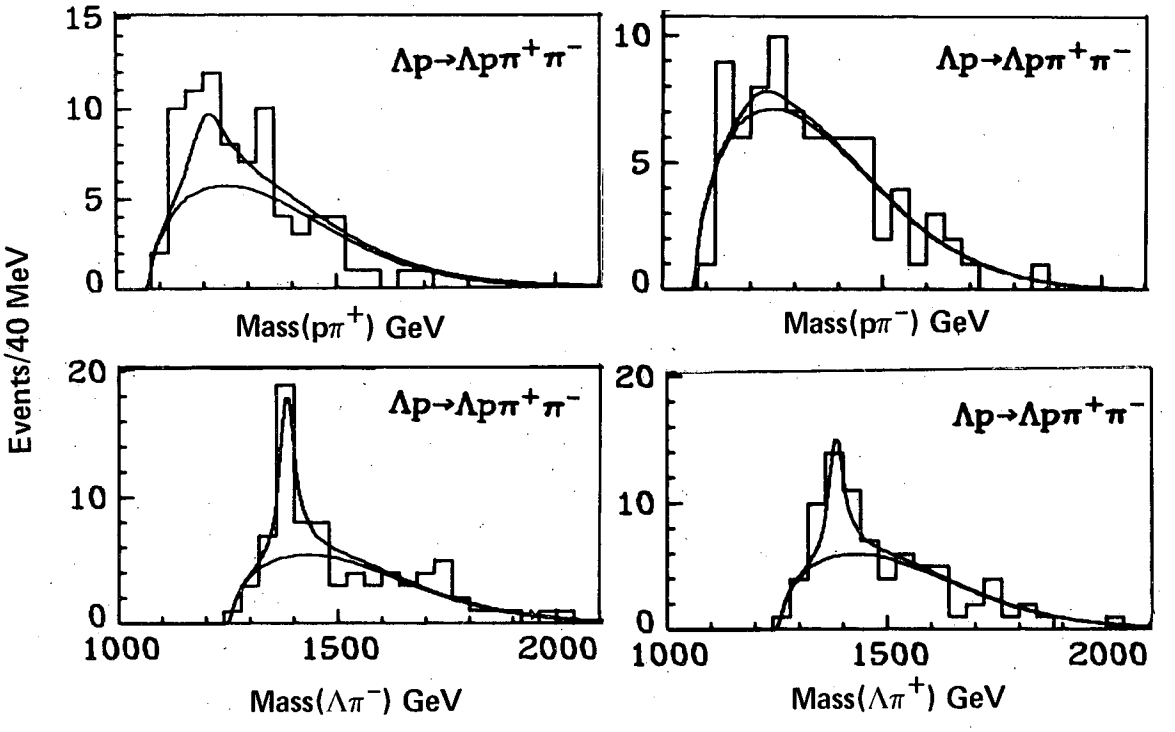

Fig. 16

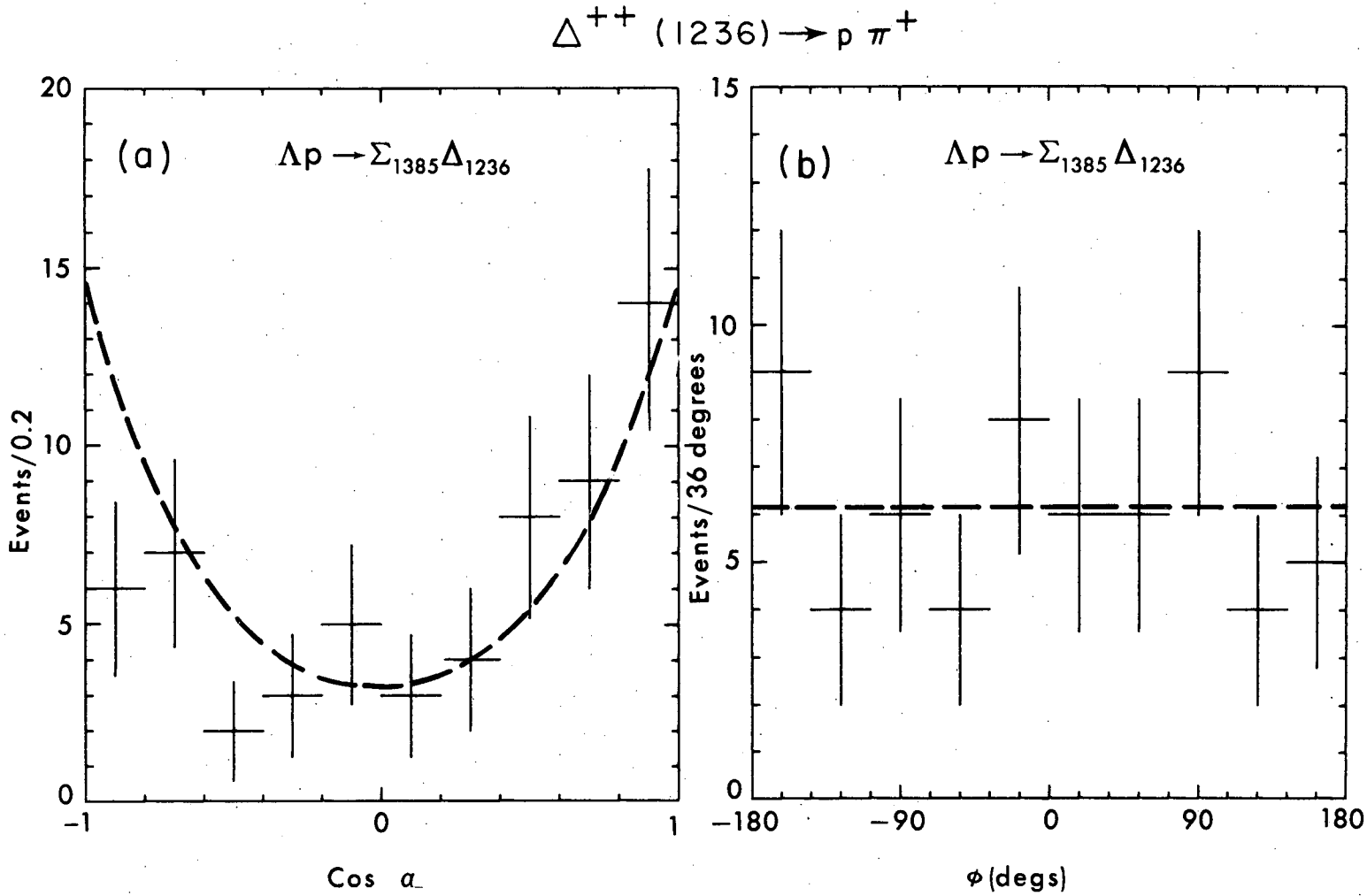

Fig. 17

XBL 747-1114A

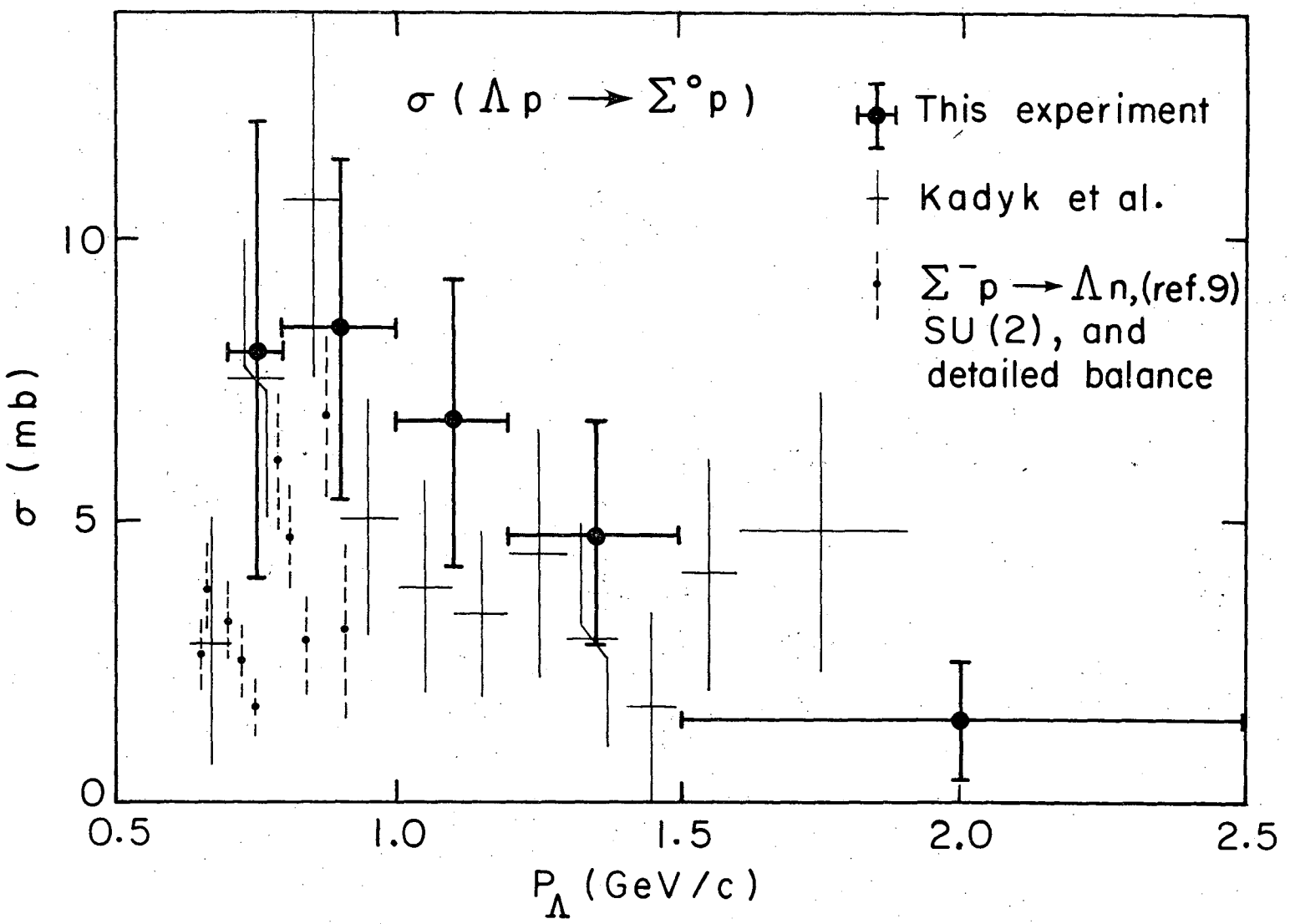

XBL 765-2889

Fig. 18

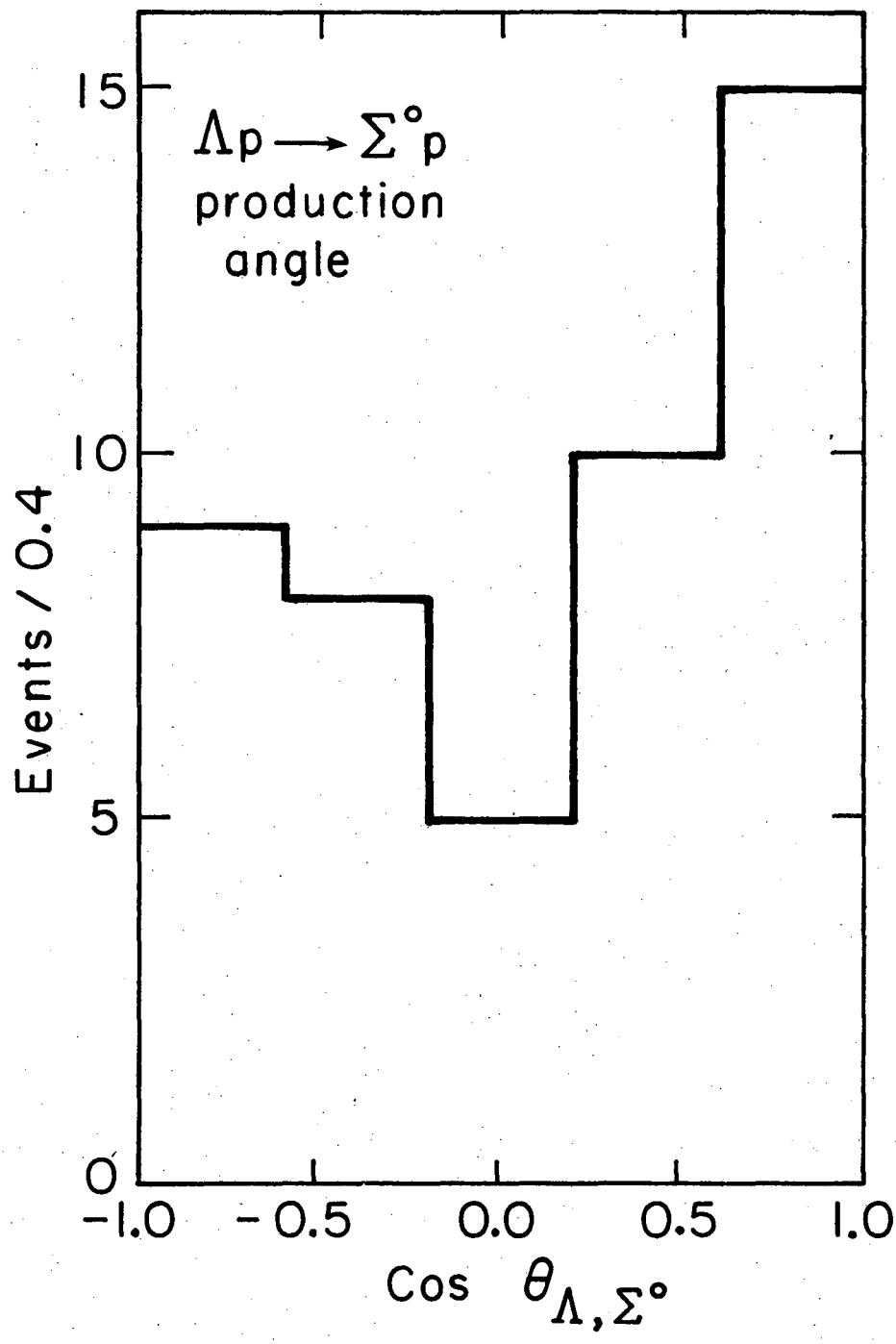

XBL 765-2887

Fig. 19

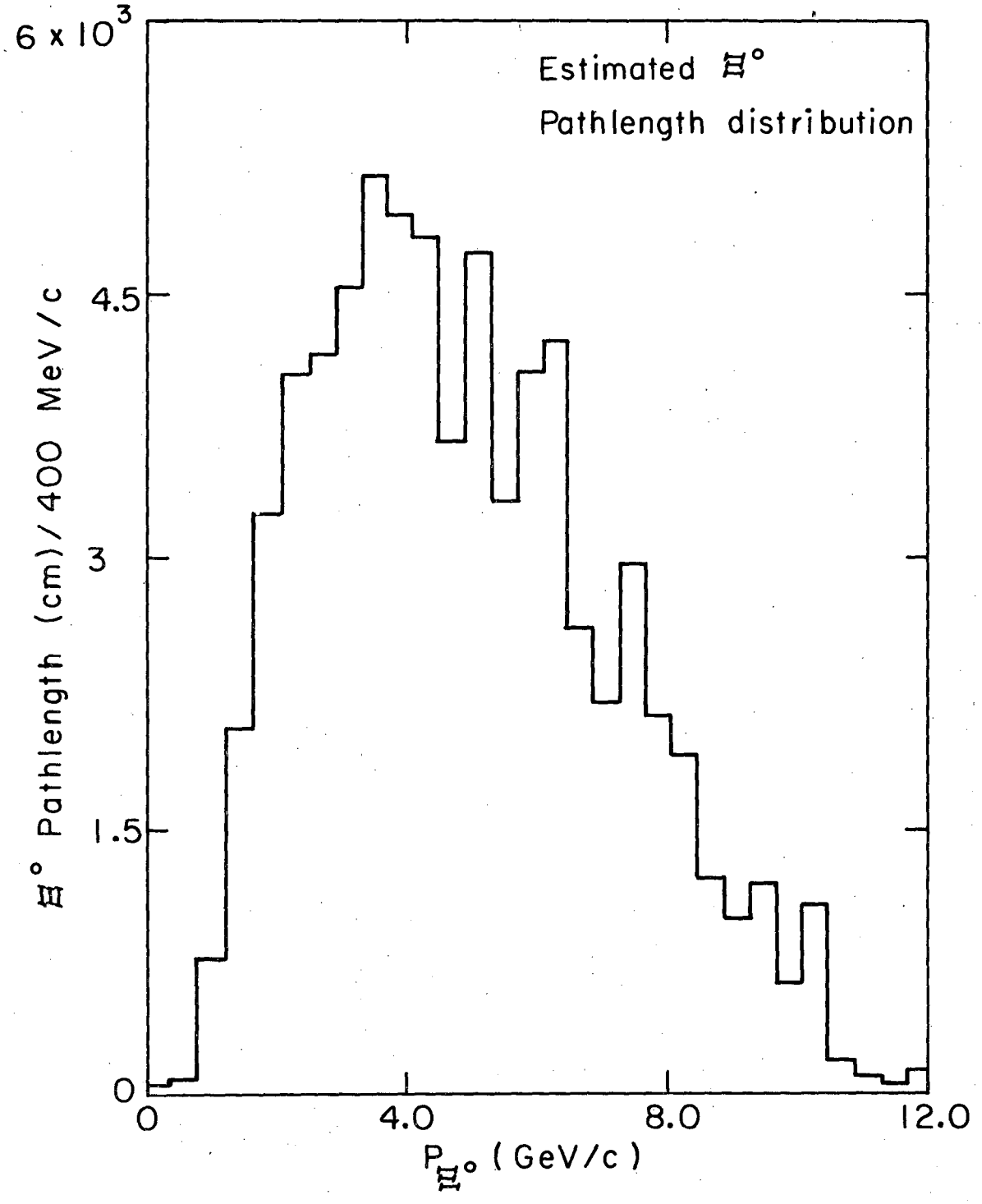

XBL 765 2886

Fig. 20

TECHNICAL INFORMATION DIVISION
LAWRENCE BERKELEY LABORATORY
UNIVERSITY OF CALIFORNIA
BERKELEY, CALIFORNIA 94720